S. Huang, Y. Ye, X. Han, W. Zuo, X. Zhang, L. Jiang 2019. “Performance evaluation of heating tower heat pump systems over the world.” Energy Conversion and Management, 186, pp. 500-515. DOI: 10.1016/j.enconman.2019.03.003

Performance evaluation of heating tower heat pump systems over the world

Shifang Huang[a, b], Yunyang Ye[b], Xu Han[b], Wangda Zuo[b], Xiaosong Zhang[a, *], Li Jiang[c]

[a] School of Energy and Environment, Southeast University, Nanjing, 210096, PR China

[b] Department of Civil, Environmental and Architectural Engineering, University of Colorado Boulder, Boulder, CO 80309, U.S.A.

[c] Nanjing TICA Climate Solutions Co., Ltd, Nanjing, 210046, PR China

* Corresponding author. E-mail address: rachpe@seu.edu.cn (Xiaosong Zhang)

Abstract: Heating tower heat pumps (HTHPs) are proposed as an alternative to the conventional heat pumps. However, lacking performance evaluation of the HTHPs in different regions limits their applications worldwide. To address this issue, this paper carries out a large-scale comprehensive performance evaluation of the HTHPs in 869 typical locations. These locations are in the warm, mixed, and cool climate zones, where buildings need both cooling and heating supply. Seven performance indices are adopted, including the annual coefficient of performance (COP), COP in cooling season, COP in heating season, regeneration ratio, number of unsatisfactory hours, matching degree of heat pump, and matching degree of heating tower. The performance evaluation of the HTHPs is conducted by the processes of location selection, building load calculation, system sizing, simulation, and evaluation. The results show that the HTHPs have excellent performance in the warm and mixed climate zones, where the average annual COPs are 4.67 and 3.68, respectively. The HTHPs are also applicable in the cool climate zone with an average annual COP of 3.11. The distributions of all the performance indices are presented through color maps, and the results are analyzed considering the air temperature and relative humidity data of the locations.

Key words: heating tower heat pump; performance evaluation; locations; application; worldwide; coefficient of performance

1. Introduction

Chillers and boilers, air-source heat pumps (ASHPs), and ground-source heat pumps (GSHPs) are widely used in the regions where buildings need both cooling and heating supply. Chillers have excellent performance in summer, but they lie idle in winter and boilers are required to satisfy the heating load. However, the boilers can do harm to the environment. The ASHPs, which can provide both cooling and heating, are becoming the most popular approach because they can be conveniently installed and maintained. But low efficiency in summer and frosting issue in winter significantly reduce its annual performance[1]. Su et al.[2] and Wang et al.[3] proposed a novel frost free ASHP, which adopted liquid desiccant to reduce the humidity ratio of the air flowing through the heat exchangers. However, this method can increase energy consumption and investment, and the issue of low efficiency in summer remains unsolved. The GSHPs have high performance in both summer and winter, however, they are subject to topographical conditions and relatively high initial cost[4]. To address these issues, heating tower heat pumps (HTHPs), as novel integrated heating and cooling units, have been proposed as an alternative to the conventional heat pump systems. The HTHPs have the advantages of high cooling efficiency similar to water chiller and cooling tower systems in summer. In winter, the HTHPs replace the boilers by using ambient air as a low-potential heat source, which improves facility utilization ratio and energy efficiency. In addition, the HTHPs address the frosting issue substantially, and they are easy to install like the ASHPs without the limitation of topographical conditions[5].

The previous studies focus more on the mechanism of the components of the HTHP systems, such as heating towers and regeneration devices. Tan et al.[6] made a revision on the Merkel's equation of standard cooling towers to calculate the thermal characteristics of a heating tower, which is also named as reversibly used water cooling tower in their study. Fujita et al.[7][8] developed a overall enthalpy transfer model for both counter and cross flow heating towers, and figured out the overall enthalpy transfer coefficients by experiments. Lu et al.[9] developed a coupled heat and mass transfer model for the heating tower. By combining this model and the experimental data, Wen et al.[10] figured out the heat transfer coefficient of a open-type heating tower by assuming Lewis number equal to one. Then, Huang et al.[11] carried out a more detailed experimental investigation and presented the influence of the inlet air/solution parameters on the performance of the heating tower. In addition, the coupled heat and mass transfer coefficients were calculated and correlation expressions were developed in this study. Song et al.[12] conducted a similar study on a closed-type heating tower, and compared the results with the heat and mass transfer process in the liquid desiccant field. Cui et al.[13][14] experimentally studied the performance of upward and downward spraying heating towers, and found they had higher heating efficiency than the ones using gravity distribution. As for the numerical studies on the performance of heating tower, both Wu et al.[15] and Zendehboudi [16] proposed an artificial neural network model. The results in their studies are in good agreement with the experimental data. Since the heating towers can absorb water vapor from the ambient air, the regeneration devices are necessary to achieve mass balance. Liang et al.[17] and Huang at al.[18] found that the heating tower can achieve self-regeneration in warm and dry working conditions. Huang at al.[5] further proposed that the main reason of the self-regeneration lies in the energy storage characteristic of the solution, and a good amount of regeneration energy can be saved by taking full advantage of the self-regeneration process. However, the self-regeneration is subjected to the weather condition. To address this problem, Ai et al.[19] proposed a mechanical vapor recompression approach, and Wen at al.[20] investigated a vacuum boiling and condensation approach. Both approaches were found to be more efficient than the conventional evaporation regeneration approaches because they utilized the condensing heat of water vapor.

The HTHPs have shown advantages over the conventional building cooling and heating systems in some pilot studies in a few cities. However, their performances have not been systemically evaluated for potential applications worldwide. Although several experimental studies are related to the system performance (summarized in Table 1), there are limitations for the evaluations: (1) each study was carried in a specific location in China; (2) there were huge differences in components and capacities in different studies; (3) the experiments were conducted under only one weather condition or small ranges of temperature and relative humidity; (4) only coefficient of performance in heating season, COP_h, was adopted for evaluation. A large-scale comprehensive performance evaluation of HTHPs would help identify their application potential in more regions. However, when conducting such large-scale evaluation, the research should meet the following requirements: (1) the locations should be selected over the world; (2) the HTHP systems should be designed and sized under the same standard; (3) the HTHP systems should be running for a calendar year, which includes both cooling and heating seasons, and consider the part load ratio of the systems; (4) the indices should be able to present the performance comprehensively, including the COP in cooling season, COP in heating season, mean COP in one year, and regeneration ratio.

Table 1. Summary of studies on system performance of HTHPs

Literature	**Location**	**Tower type**	**Solution**	**Compressor**	**Heating capacity**	**Outdoor weather**	COP_h
Liang et al.[21]	Nanjing	Open-type	Glycol	Rotor	5 kW	T_a=-2℃	[2.72, 3.02]
Wu et al.[22]	Changsha	Open-type	$CaCl_2$	Screw	125 kW	T_a=4.6℃, φ_a=90%	[2.70, 2.86]
Zhang et al.[23]	Nanjing	Open-type	Glycol	Rotor	7 kW	T_a=6.5℃, φ_a=76%	3.02
Li et al.[24]	Changsha	Closed-type	Urea	Screw	125 kW	T_a=[-1, 5]°C, φ_a=[71%, 95%]	[2.58, 3.90]
Cheng et al.[25]	Changsha	Closed-type	/	Scroll	809 kW	T_a=4.3℃, φ_a=93.9%	3.00
Chen et al.[26]	Hangzhou	Open-type	/	Screw	/	T_a=[-3, 4] ℃	[3.00,3.73]

To address the above problems, this paper carries out a large-scale comprehensive performance evaluation of the HTHPs over the world. Firstly, the HTHP model is developed and validated. Then, the performance evaluation of the HTHPs is implemented by the processes of location selection, building load calculation, system sizing, simulation, and evaluation. Seven performance indices are proposed and adopted to carry out a comprehensive evaluation. Finally, all the results are presented through color maps, and the distributions are analyzed by using air temperature and relative humidity data of the locations.

2. System description and modeling

2.1. Description of HTHP system

Fig. 1 demonstrates the schematics of a typical HTHP system, including a heating tower, a heat pump, a regeneration device, a solution tank, four pumps, and eight valves. In the cooling season, the HTHP system works as a chiller with a cooling tower, with valves 1-4 open and valves 5-8 closed. The evaporator of the heat pump is connected with user sides supplying chilled water to the buildings. The condenser of the heat pump is coupled with the heating tower, in which water is adopted and evaporates in the tower to reject heat to the ambient air. Make-up water is added to this loop to achieve mass balance. The regeneration loop, including the regeneration device, solution tank, and solution pumps, is shut down in the cooling season.

In the heating mode, valves 5-8 are open, while valves 1-4 are closed. The condenser of the heat pump supplies hot water to the building. The evaporator is connected to the heating tower for absorbing heat from the ambient air. In this loop, solution with low freezing point (e.g. glycol aqueous, calcium chloride aqueous) is adopted instead of water to avoid system freeze. In some conditions, the solution may absorb both heat and mass from the ambient air. As a result, the solution becomes diluted, which increases risks of system freeze. To address this problem, a regeneration device based on vacuum boiling and condensation is employed to achieve mass balance[20]. The solution tank is equipped to store dilute solution temporarily in the heating season to make full use of the self-regeneration process. Also, it is used for solution storage in the cooling and transition seasons.

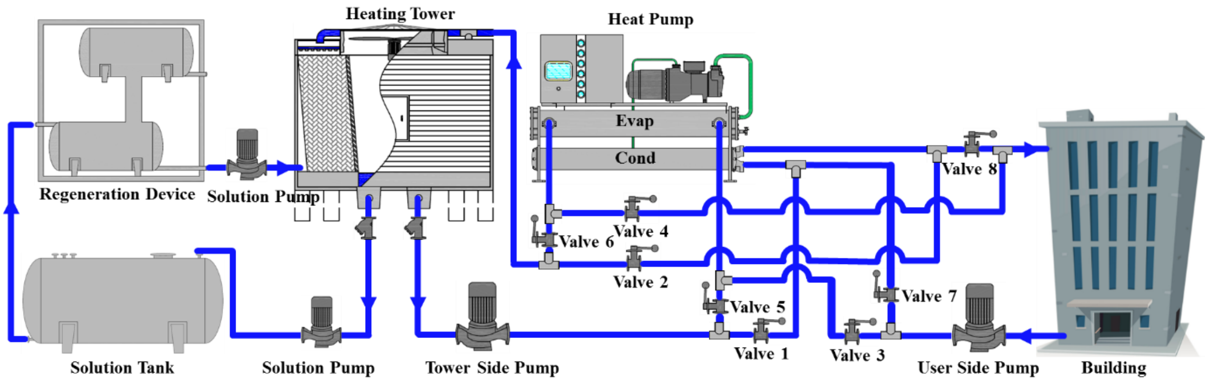

Fig. 1. The schematic of the HTHP system

2.2. Modeling of HTHP system

The models for all the components of the studied HTHP system are developed separately, and then coupled by balancing heat, mass and energy between different components. The following sections describe the models for the heat pump, heating tower, and regeneration device, respectively.

2.2.1. Heat pump model

The heat pump consists of four main components, including the screw compressor, shell-tube evaporator, shell-tube condenser, and thermostatic expansion valve. Models of the components are developed as follows.

Compressor

The refrigerant mass flow rate, M_R, and power consumption, W_{comp}, for screw compressors can be expressed by a function of the evaporating temperature, T_e, and condensing temperature, T_c [27], and rotation speed N_{comp} [28][29]:

$$M_R = (\alpha_1 + \alpha_2 T_e + \alpha_3 T_c + \alpha_4 T_e^2 + \alpha_5 T_e T_c + \alpha_6 T_c^2 + \alpha_7 T_e^3 + \alpha_8 T_e^2 T_c + \alpha_9 T_e T_c^2 + \alpha_{10} T_c^3)\frac{N_{comp}}{N_{comp,rated}}, \tag{1}$$

$$W_{comp} = (\beta_1 + \beta_2 T_e + \beta_3 T_c + \beta_4 T_e^2 + \beta_5 T_e T_c + \beta_6 T_c^2 + \beta_7 T_e^3 + \beta_8 T_e^2 T_c + \beta_9 T_e T_c^2 + \beta_{10} T_c^3)\frac{N_{comp}}{N_{comp,rated}}, \tag{2}$$

where the subscript $rated$ represents the performance under rated speed. The α_{1-10} and β_{1-10} are coefficients regressed from experimental data provided by manufacturer BITZER.

Evaporator and condenser

The classical logarithmic mean temperature difference method is adopted in both evaporator and condenser models. The cooling capacity of the evaporator, Q_e, and the heating capacity of the condenser, Q_c, can be expressed as follows:

$$Q_e = K_e A_e LMTD_e \quad , \tag{3}$$

$$Q_c = K_c A_c LMTD_c \quad , \tag{4}$$

where K, A, and $LMTD$ are the heat transfer coefficient, heat transfer area, and logarithmic mean temperature difference between refrigerant and water/ solution. The subscript e represents the evaporator, and c represents the condenser.

The overall heat transfer coefficient for the evaporator or condenser, K_e (K_c), can be expressed as a function of the heat transfer coefficient inside the tube, K_i, and outside the tube, K_o:

$$K_e\ (K_c) = \frac{1}{\left(\frac{1}{K_i}+R_i\right)\frac{A_O}{A_i}+\frac{\delta A_O}{\lambda_{wall}A_m}+R_O+\frac{1}{K_O}} \quad , \tag{5}$$

where R is the heat transfer resistance. The δ is the thickness of the wall. The subscripts i and o represent the property inside and outside the tube, respectively. And the subscripts m is the mean value of the inside and outside property. The heat transfer coefficients for the evaporation of R22 inside the tube, condensation of R22 outside the tube, and water/solution across the tube can be found in our pervious studies[5].

The heat transfer capacities of the evaporator and condenser can be expressed by the energy variations of refrigerant and water/solution.

$$Q_e = M_R(h_1 - h_4) \quad , \tag{6}$$

$$Q_e = Cp_w M_{chw}(T_{chwr} - T_{chws}) \text{ or } Q_e = Cp_s M_s (T_{ss} - T_{sr}) \quad , \tag{7}$$

$$Q_c = M_R(h_2 - h_3) \quad , \tag{8}$$

$$Q_c = Cp_w M_{cw}(T_{cwr} - T_{cws})\ or\ Q_c = Cp_w M_{hw}(T_{hws} - T_{hwr}) \quad , \tag{9}$$

where h_1 and h_4 are the enthalpy of the refrigerant in the outlet and inlet of the evaporator, h_2 and h_3 are the enthalpy of the refrigerant in the inlet and outlet of the condenser.

Expansion valve

The expansion process in the expansion valve is taken as an isenthalpic process as shown in Eq.(10). The mass flow rate of the refrigerant can be calculated[30]:

$$h_3 = h_4 \quad , \tag{10}$$

$$M_R = C_D A_{th}\sqrt{\rho_{R,l}\,(P_c - P_e)} \quad , \tag{11}$$

where, C_D is the constant mass flow coefficient. The A_{th} represents the geometric throat area of the thermostatic expansion valve, which is adjustable and controlled by the superheat. The P_c and P_e are the pressure of condenser and evaporator, respectively.

2.2.2. Heating tower model

The heating tower model in winter is developed using a finite difference method[11][18]. Eqs.(12) and (13) express the energy and mass balances between air and solution. Eq.(14) describes the solute balance of the solution.

$$m_a dh_a = -Cp_s m_s dT_s - Cp_s T_s dm_s \quad , \tag{12}$$

$$dm_s = -m_a d\omega_a \quad , \tag{13}$$

$$X_s m_s = (X_s + dX_s)(m_s + dm_s) \quad , \tag{14}$$

where dh_a is the enthalpy variation of the air through an element. The dT_s, dm_s and dX_s represent the variations of the solution in temperature, mass flow rate and concentration through an element, respectively. The X_s is the mass concentration of the solution.

The convective heat and mass transfer are also applied as follows:

$$h_c L \cdot dx \cdot dy \cdot \alpha_w (T_s - T_a) = m_a (Cp_a + \omega_a Cp_v) dT_a \quad , \tag{15}$$

$$h_d L \cdot dx \cdot dy \cdot \alpha_w (\omega_s - \omega_a) = m_a d\omega_a \quad , \tag{16}$$

where ω_s is the equivalent humidity ratio of the solution, dT_a and $d\omega_a$ are the temperature and humidity ratio variation of air through an element. The $dx \cdot dy$ represents the size of each element, L is the length of the packing, and α_w is the specific area of the packing. The h_c is the heat transfer coefficient, h_d is the mass transfer coefficient. These two coefficients are expressed as functions of the solution mass flow flux, G_s, and air mass flow flux, G_a:

$$h_c = \gamma_1 G_s^{\gamma_2} G_a^{\gamma_3} \quad , \tag{17}$$

$$h_d = \xi_1 G_s^{\xi_2} G_a^{\xi_3} \quad , \tag{18}$$

The coefficients γ_{1-3} and ξ_{1-3} are regressed from experimental data of our previous study[11].

By replacing the subscript s by w and setting X_s to zero, the model listed above can also be used to simulate the performance of heating tower in cooling season. The heat and mass transfer capacities in both cooling and heating seasons can be expressed as follows:

$$Q_{sh} = (Cp_a + \omega_a Cp_v) \cdot M_a \cdot (T_{a,o} - T_{a,i}) \ , \tag{19}$$

$$Q_{lh} = r_v \cdot M_a \cdot (\omega_{a,o} - \omega_{a,i}) \ , \tag{20}$$

where Q_{sh} is the sensible heat transfer capacity, and Q_{lh} is the latent heat transfer capacity. Here, the positive values of Q_{sh} and Q_{lh} mean that the heat and mass transfer directions are from air to condenser water or solution. When the values are negative, the directions are the opposite. The Cp, M, T, ω, and r represent the specific heat, mass flow rate, temperature, humidity ratio, and vaporization latent heat, respectively. The subscripts a, v, i, and o represent the air, water vapor, tower inlet, and tower outlet, respectively.

2.2.3. Regeneration model

A regeneration module based on vacuum boiling and condensation is adopted in this study to satisfy the regeneration demand in winter. The adopted module approximates the efficiency of the regeneration system, η_{RD}, as a constant of 3.4 kg/kWh[20]. This is because the performance of this regeneration method is independent of the weather conditions. Then the power input for the regeneration, W_{RD}, can be calculated by the following equation:

$$W_{RD} = \frac{\int \frac{Q_{lh}}{r_w} dt}{\eta_{RD}} \quad . \tag{21}$$

2.3. Validation of models

The physics-based model developed in this study is validated using our experimental data[5], as shown in Fig. 2. The relative error is within ±10% for all the predicted values, and the average error is 3.48% for cooling/heating capacity, and 3.05% for the COP. This indicates that the physics-based model has high accuracy in predicting the performance of the HTHP. However, in most experimental runs, the predicted cooling/heating capacity is a little bit higher than the experimental capacity. There are two reasons: 1) In our models, the heat exchangers and pipelines are well adiabatic, while the real system can not reach 100% adiabatic condition. Therefore, there is some heat leakage from the hot water to the surroundings in the winter condition, and some heat absorption from the surroundings to the chilled water in the summer condition. 2) The real system has dirt in the heat exchangers, which can weaken the heat transfer process. Therefor, the experimental cooling/heating capacity can be less than the predicted capacity.

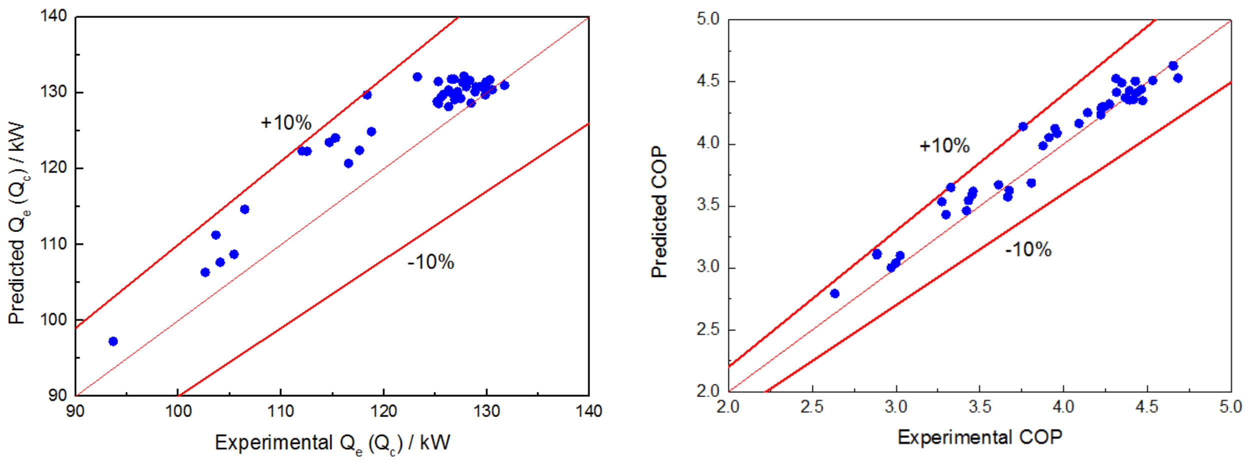

(a) Cooling/heating capacity (b) COP

Fig. 2. Comparison between the experimental data and the model prediction of the HTHP

3. Performance evaluation of HTHP systems

The performance evaluation of HTHPs over the world is carried out by the steps of location selection, building load calculation, system sizing, simulation, and evaluation, as shown in Fig. 3. The location selection step is to determine the potential thermal climate zones (locations) for HTHPs' application. The building load calculation and system sizing steps are conducted to provide input parameters for system simulations in different locations. In the simulation step, hourly simulation for each case is carried out by coupling weather, building, and HTHP system. In the evaluation step, seven performance indices are proposed to realize a comprehensive evaluation. The details of all the steps will be demonstrated in the following sections.

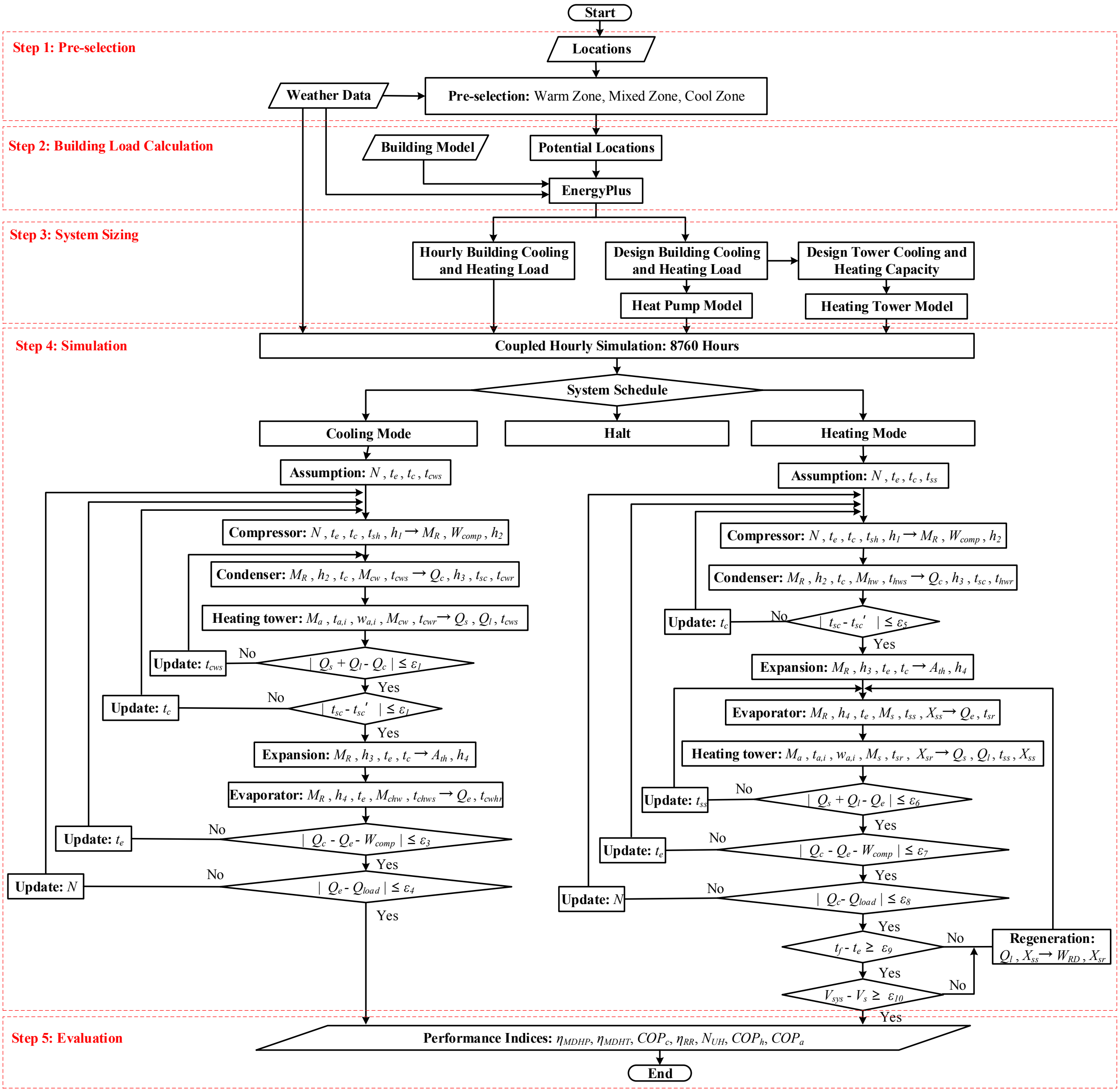

Fig. 3. Flow chart of the performance evaluation of HTHPs over the world

3.1. Selection of Locations

The location selection process is carried out first to exclude the regions which are clearly unsuited for the application of the HTHPs. To determine the thermal climate zones for locations over the world, cooling degree-day base 10°C (CDD10°C) and heating degree-day base 18°C (HDD18°C) are adopted, according to ANSI/ASHRAE Standard 169-2013[31]:

$$\mathrm{CDD10°C} = \sum_{day=1}^{365} \max\left(\left(\frac{1}{24}\sum_{hr=1}^{24} T_a - 10\right), 0\right) \ , \tag{22}$$

$$\mathrm{HDD18°C} = \sum_{day=1}^{365} \max\left(\left(18.3 - \frac{1}{24}\sum_{hr=1}^{24} T_a\right), 0\right) \ . \tag{23}$$

According to the ranges of the CDD10°C and HDD18°C, nine thermal climate zones are defined, including Zone 0 (extremely hot), Zone 1 (very hot), Zone 2 (hot), Zone 3 (warm), Zone 4 (mixed), Zone 5 (cool), Zone 6 (cold), Zone 7 (very cold), and Zone 8 (subarctic/arctic), as shown in Fig. 4. The buildings in Zones 0-2 only require cooling supply, which can be satisfied by chillers. Similarly, boils are suitable for the buildings in Zones 6-8, which only require heating supply, and heat pumps have poor performance in such cold regions. Zones 3-5, where buildings need both cooling and heating supply, are considered as the potential regions for the application of HTHPs.

Weather data for 2,581 locations is downloaded from EnergyPlus website (https://energyplus.net/weather). Then, the CDD10°C and HDD18° for all the locations are calculated. After the selection process, 869 locations in Zones 3-5 are left, as presented in Fig. 4. Most locations are in China (50, 34, 36 locations in Zones 3-5, respectively), the USA (169, 155, 180 locations in Zones 3-5, respectively), and Europe (69, 50, 38 locations in Zones 3-5, respectively). The other locations are in the rest of the world (65, 17, 6 locations in Zones 3-5, respectively), such as Japan, Australia, and Argentina. The distribution of selected locations is demonstrated in Fig. 5.

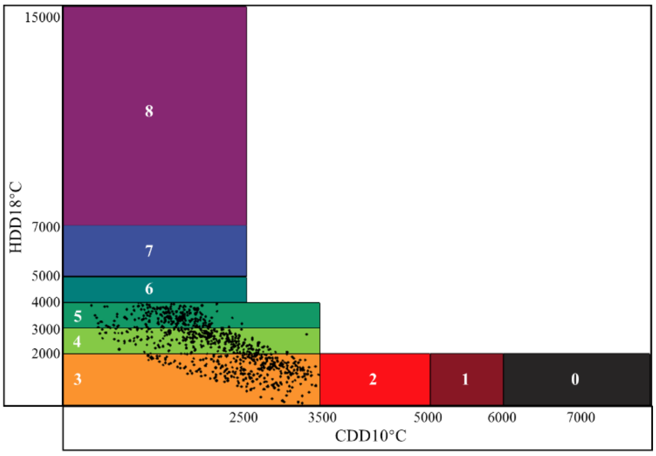

Fig. 4. Thermal climate zones

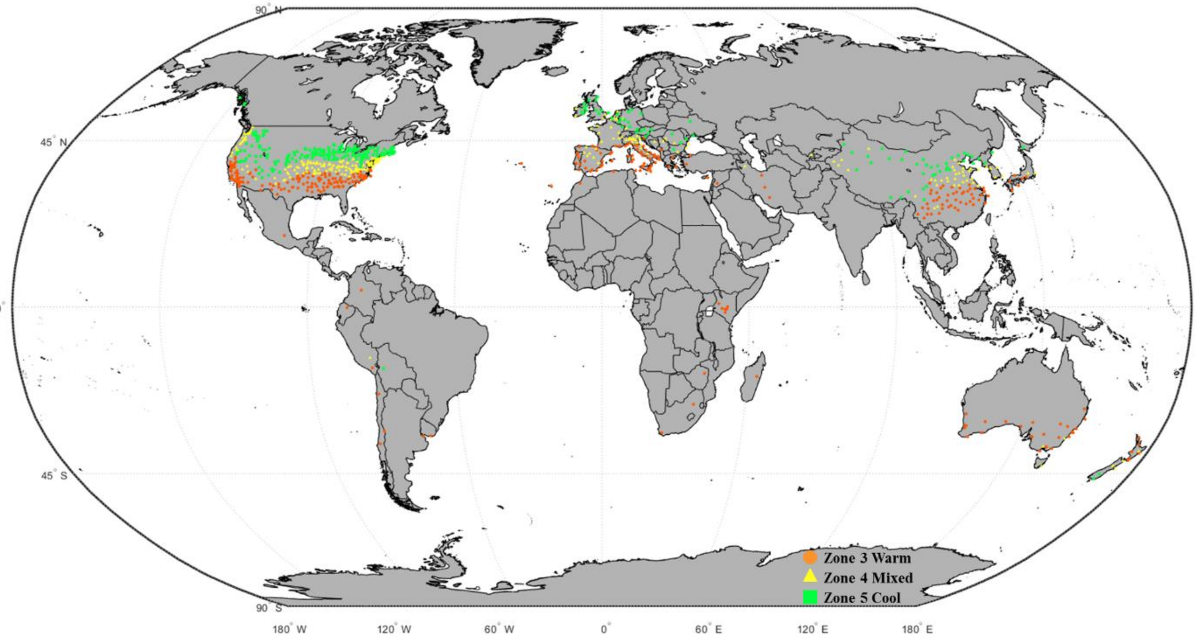

Fig. 5. Distribution of selected locations over the world

3.2. Building load calculation

In the building load calculation process, reference office building models developed by U.S. Department of Energy (DOE) are adopted. These reference building models are complete descriptions for whole building energy analysis, and organized by climate zones (here, A represents the humid zone, B represents the dry zone, and C represents the marine zone[31]). The reference buildings have the same shape and architecture, as shown in Fig. 6. The details of the settings of envelop, occupancy, and equipment, are demonstrated in Table 2.

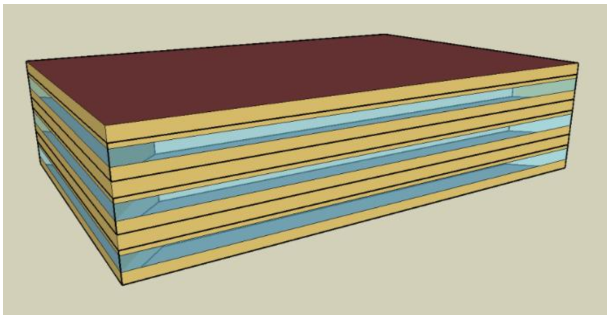

Fig. 6. Building shape and architecture

Table 2. Building characteristics in different climate zones

Building characteristics		Climate zones							
		3A	3B	3C	4A	4B	4C	5A	5B
1 General information									
Total floor area	m^2	4,982							
Cooling indoor set point	°C	24							
Heating indoor set point	°C	21							
Indoor RH	%	60							

2 Building envelope									
R-value of exterior wall	m^2 K W^{-1}	1.36	1.10	1.36	1.98	1.76	1.92	2.15	2.15
R-value of roof	m^2 K W^{-1}	2.44	3.66	2.00	3.03	2.99	2.75	3.38	3.51
U-value of windows	W m^{-2} K^{-1}	4.09	5.84	4.09	3.35	4.09	4.09	3.35	3.35
SHGC of windows	/	0.26	0.25	0.39	0.36	0.36	0.39	0.39	0.39
Window-to-wall ratio	/	0.33							
3 Zone summary									
Occupant density	(m^2 $person^{-1}$)	18.58							
Ventilation rate	(l s^{-1} $person^{-1}$)	10							
Lighting load	(W m^{-2})	16.90							
Equipment load	(W m^{-2})	10.76							
Infiltration rate	(ACH)	Perimeter: 0.98-1.03; Mid-floor:0.41; Top-floor: 3.76							

Based on the reference building models and settings mentioned above, we used Python to call EnergyPlus to calculate the building loads for the 869 locations. Building loads are used as input data for the system sizing, simulation, and evaluation, which will be presented in Sections 3.3 to 3.5.

3.3. Design and sizing of HTHP system

A series of heat pumps are designed to satisfy the different building loads of the 869 locations. In the nominal cooling condition, the supply and return chilled water temperature are 7 and 12°C, and the supply and return cooling water temperature are 30 and 35°C. In the nominal heating condition, the supply and return solution temperature are -1 and 1.5°C, and the supply and return hot water temperature are 40 and 45°C. The cooling and heating capacities, COP_c, and COP_h in the nominal cooling and heating conditions are presented in Table 3.

Table 3. Parameters of designed heat pumps in nominal conditions

Heat pump type	Cooling capacity	Heating capacity	COP_c	COP_h
	kW	kW	/	/
HEZEHP080CSH	81	73	4.22	3.39
HEZEHP100CSH	100	92	4.20	3.44
HEZEHP140CSH	135	121	4.28	3.37
HEZEHP160CSH	155	139	4.32	3.40
HEZEHP190CSH	187	171	4.29	3.44
HEZEHP200CSH	203	184	4.38	3.52
HEZEHP210CSH	215	197	4.34	3.46
HEZEHP250CSH	254	230	4.51	3.55
HEZEHP280CSH	281	256	4.43	3.52
HEZEHP320CSH	319	291	4.43	3.52
HEZEHP380CSH	380	343	4.48	3.53
HEZEHP440CSH	440	396	4.58	3.65
HEZEHP510CSH	505	461	4.59	3.66
HEZEHP570CSH	574	523	4.61	3.67

In addition, a series of heating towers are designed to satisfy the different heat rejection and absorption capacities of the heat pumps. In the nominal cooling condition, the air dry/wet-bulb temperature is 32°C/28°C, the air/water flow flux of the heating tower is 2 kg m^{-2} s^{-1}/4 kg m^{-2} s^{-1}, and the supply and return cooling water temperature are 30 and 35°C. In the nominal heating condition, the air dry/wet-bulb temperature is 7°C/6°C, the air/water flow flux of the heating tower is the same as that in cooling condition, the supply and return solution temperature are -1 and 1.5°C. In this study, we adopt glycol aqueous as working fluid in heating condition, and its concentration is 15% in the nominal condition. The parameters of the designed heating towers, including heat rejection and absorption capacities, air and water (solution) mass flow rates, are demonstrated in Table 4.

Table 4. Parameters of designed heating towers in nominal conditions

Heating tower type	Heat rejection capacity	Heat absorption capacity	Water/solution flow rate	Air flow rate
	kW	kW	m^3 h^{-1}	m^3 h^{-1}
HEZEHT130060	132	55	22	24,925
HEZEHT200080	198	82	33	37,388
HEZEHT260110	264	109	44	49,850
HEZEHT330140	330	136	55	62,313
HEZEHT400160	396	164	66	74,776
HEZEHT460190	462	191	77	87,238
HEZEHT530220	528	218	88	99,701
HEZEHT590250	594	246	99	112,164
HEZEHT660270	660	273	110	124,626
HEZEHT730300	726	300	121	137,089
HEZEHT790330	793	328	132	149,551
HEZEHT860360	859	355	143	162,014
HEZEHT930380	925	382	154	174,477
HEZEHT990410	991	409	165	186,939

After the design of the heat pumps and heating towers, the sizing of the HTHPs for different cases can be done with the calculated building loads. Here, we give two examples to show the sizing process. For city Wuhan, China, the designed building cooling/heating load is 411 kW/253 kW, and the corresponding tower heat rejection/absorption load is 500 kW/184 kW. Therefore, heat pump HEZEHP440CSH (440 kW/396 kW) and heating tower HEZEHT530220 (528 kW / 218 kW) are selected to satisfy both cooling and heating demand. For city Beijing, China, the designed building cooling/heating load is 369 kW/297 kW, and the corresponding tower heat rejection/absorption load is 451 kW/213 kW. So, heat pump HEZEHP380CSH (380 kW/343 kW) and heating tower HEZEHT530220 (528 kW / 218 kW) are selected.

3.4. Simulation of HTHP system

The weather data, building loads, and system parameters of the selected 869 locations obtained by Steps 1-3 are inputs of Step 4 (simulation). For each location, the simulation of 8,760 hours in one calendar year is carried out, as shown in Fig. 3. According to the building schedule, the modes of the HTHP is selected first, including cooing, heating, and halt modes. Then, the models of the components mentioned in Section 2.2 are implemented in the MATLAB environment. To solve the non-linear models which are linked by energy and mass balances, a newton iterative method is applied. In the cooling mode, the rotation speed of the compressor, evaporating temperature, condensing temperature, and cooling water supply temperature are selected as iteration variables. The newton iteration is used to update the iteration variables according to the energy and mass balances between outdoor air, cooling water, refrigerant, and chilled water. In this paper, the superheating and subcooling values are both set as 5° C. In the real system, we adjust the geometric throat area of the thermal expansion valve, A_{th}, to make sure that the superheating value reaches its set point. But the A_{th} has a physical constraint, which can only be adjusted from 0% to the 100% opening. So, we also calculate and record the A_{th} in the 'Expansion' module. In the most conditions, the A_{th} is in the above range since we select appropriate thermostatic expansion valves for all the heat pumps listed in our manuscript. In some extreme condition when the A_{th} exceeds the maximum value, we set the A_{th} as the maximum value, and then set the superheating value as an unknown. In the heating mode, the cooling water is replaced by glycol aqueous as the working fluid in the heating tower, and chilled water is replaced by hot water. In addition, the regeneration device is coupled with the evaporator and heating tower. As mentioned in Section 2.1, the heating tower absorbs both heat and mass (water) from the ambient air in some conditions. Fortunately, the heating tower is also able to evaporate the excessive water when the water vapor pressure of the solution is higher than that of the air[18]. This process named as "self-regeneration" can reduce the regeneration load and energy consumption[5]. In order to make full use of the self-regeneration process, the regeneration device only runs when the freezing point of the solution is not low enough or the volume of the solution is larger than the storage capacity of the system. The solution with higher concentration has lower freezing point, which can prevent system from freeze and improve the system safety. However, the increase of concentration can also reduce the water vapor pressure of the solution, which means that the solution will absorb more latent heat from the ambient air. As a result, the energy consumption of the regeneration device will increase significantly. So, the ideal state is keeping the safety margin close to 0 °C, which is the difference between the solution temperature in the outlet of the evaporator and the freezing point of the solution. In this study, by considering the measuring error and system response time in the real project, we set the safety margin as 3 °C.

3.5. Evaluation of HTHP system

As indicated in the introduction, only COP_h was adopted for evaluation of HTHP' operational performance in heating season in the previous studies. However, more performance indices are required in the designing and evaluating process of a building's cooling and heating system. For instance, there are three alternatives for a real project: chiller and boiler, ASHP, and HTHP. Commonly, we need to compare the initial cost and annual energy consumption to carry out the economic analysis. Besides the COP_h, we still need to know the coefficient of performance of the HTHP in cooling season, the required capacity and energy consumption of the regeneration device. Besides the new newly established system, the HTHP system can also be used to transformation a conventional water-cooled chiller system to satisfy both cooling and heating demands. In this case, we need to know if additional towers or heat pump hosts are required, which can have an influence on the initial cost. Therefore, we propose the matching degree of heat pump and the matching degree of heating tower to address the above problem. The detailed definitions and functions of these performance indices are listed as follows.

The matching degree of heat pump in cooling and heating modes, η_{MDHP}, is defined as:

$$\eta_{MDHP} = \frac{Q_{DBC}/Q_{DBH}}{Q_{HPC}/Q_{HPH}} \,, \tag{24}$$

where Q_{DBC} and Q_{DBH} mean the designed building cooling and heating loads, respectively. The Q_{HPC} and Q_{HPH} are the heat pump cooling and heating capacities, respectively. When η_{MDHP} is larger than 1, it indicates that the heat pump should be sized according to the cooling mode in new HTHP system, or no additional heat pumps is required in the transformation of a chiller system into a HTHP system. When η_{MDHP} is less than 1, the conclusions are the opposite.

The matching degree of heating tower in cooling and heating modes, η_{MDHT}, is defined as:

$$\eta_{MDHT} = \frac{\left(Q_{DBC}+\frac{Q_{DBC}}{COP_{c,rated}}\right)/\left(Q_{DBH}-\frac{Q_{DBH}}{COP_{h,rated}}\right)}{Q_{HTC}/Q_{HTH}} \,, \tag{25}$$

where $COP_{c,rated}$ and $COP_{h,rated}$ are the rated cooling and heating coefficients of the heat pump, respectively. The Q_{HTC} and Q_{HTH} are the heating tower cooling and heating capacities, respectively. Similarly, the heating tower should be sized to satisfy the tower cooling load in new system, or no additional heating tower is required in transformation, when η_{MDHT} is greater than 1.

The regeneration ratio in the winter conditions, η_{RR}, is define as follow:

$$\eta_{RR} = \frac{\int Q_{lh}dt}{\int (Q_{lh}+Q_{sh})dt} \,. \tag{26}$$

The η_{RR} indicates the regeneration penalization in the winter conditions. This performance index can be used to size the regeneration device, and to calculate its energy consumption.

The number of unsatisfactory hours in the winter conditions, N_{UH}, is defined as the number of hours when the heating capacity of the system cannot satisfy the building heating load:

$$N_{UH} = \int n_{UH} dt, \tag{27}$$

$$n_{UH} = \begin{cases} 1, & Q_{HPH} < Q_{BH} \\ 0, & Q_{HPH} \geq Q_{BH} \end{cases} \,, \tag{28}$$

$$W_{EH} = \int \max(Q_{BH} - Q_{HPH}, 0)dt \,, \tag{29}$$

where Q_{BH} represents the building heating load. In the unsatisfactory hours, the unsatisfied heating demands need to be provided by an auxiliary electric heater, and W_{EH} is the power consumption of the electric heater.

By considering the energy consumption of heat pump, regeneration device, and electric heater, the energy performance of the HTHP is measured by the coefficient of performance, COP:

$$COP_c = \frac{\int Cp_w M_{chw}(T_{chwr} - T_{chws})dt}{\int W_{HPC}dt} , \tag{30}$$

$$COP_h = \frac{\int Cp_w M_{hw}(T_{hws} - T_{hwr})dt}{\int (W_{HPH} + W_{RD} + W_{EH})dt} , \tag{31}$$

$$COP_a = \frac{\int Cp_w M_{chw}(T_{chwr} - T_{chws})dt + \int Cp_{hw} M_w (T_{hws} - T_{hwr})dt}{\int W_{HPC}dt + \int (W_{HPH} + W_{RD} + W_{EH})dt} , \tag{32}$$

where the subscripts c, h, a represent cooling season, heating season, and annual, respectively. The W_{HPC} and W_{HPH} are heat pump power consumptions in cooling and heating modes, respectively.

3.6. Development of color map

To demonstrate the distributions of all the performance indices for different locations, color maps are developed by combining the indices and calibrations of the color bars, as shown in Table 5. For instance, Shanghai, China is selected as the specific location, whose longitude and latitude are 121.47 and 31.40, respectively. The COP_a of Shanghai is 4.50, and its [R, G, B] matrix is between [0, 255, 255] and [255, 255, 0]. As the COP_a increases from 4.0 to 5.0, the R increases from 0 to 255, and the B decreases from 255 to 0 linearly. Therefore, we can obtain the [R, G, B] matrix by solve the following equations: (R+1) / (255+1) = COP_a- 4.0, (B+1) / (255+1) = 5.0- COP_a. So, the [R, G, B] is calculated to be [127, 255, 127]. Similarly, the [R, G, B] matrixes of all the performance indices for different locations can be obtained, and the color maps are able to be developed based on the results.

Table 5. Calibrations of color bars

Color	[R, G, B]	COP_c	η_{RR}	N_{UH}	COP_h	COP_a	η_{MDHP}	η_{MDHT}
	[0, 0, 0]	5.0	-35%	-150	2.0	2.0	0.4	0.4
	[0, 0, 255]	5.5	-20%	0	2.5	3.0	0.7	0.6
	[0, 255, 255]	6.0	-5%	150	3.0	4.0	1.0	0.8
	[255, 255, 0]	6.5	10%	300	3.5	5.0	1.3	1.0
	[255, 0, 0]	7.0	25%	450	4.0	6.0	1.6	1.2
	[0, 0, 0]	7.5	40%	600	4.5	7.0	1.9	1.4

4. Results and discussion

According to the steps indicated in Section 3, hourly simulations of the 869 locations are carried out for a whole year. Based on the results, locations which need cooling or heating supply only for a few days are excluded, such as locations in Canada, England, south Australia. Seven performance indices for the remaining 762 locations are calculated, and presented in color map.

4.1. Performance in cooling season

The COP_c of the HTHPs in cooling season vary from 5.13 to 7.40, as demonstrated in Fig. 7 to Fig. 10. Since the HTHP works like a water-cooled chiller with a cooling tower in cooling season, the COP_c is mainly influenced by the air wet-bulb temperature, which is determined the air dry-bulb temperature and relative humidity. As a result, the locations with lower air dry-bulb temperature or relative humidity have higher COP_c, such as the ones in plateaus (Colorado and Utah of the USA, Xinjiang and Gansu province of China) or with maritime climate (California of the USA, Yunnan province of China, Salamanca of Spain). In general, the COP_c increases as the latitude increase because the air dry-bulb temperature usually increases with the latitude. The average COP_c is 5.73 in Zone 3 (warm), 5.83 in Zone 4 (mixed), and 6.14 in Zone 5 (cool).

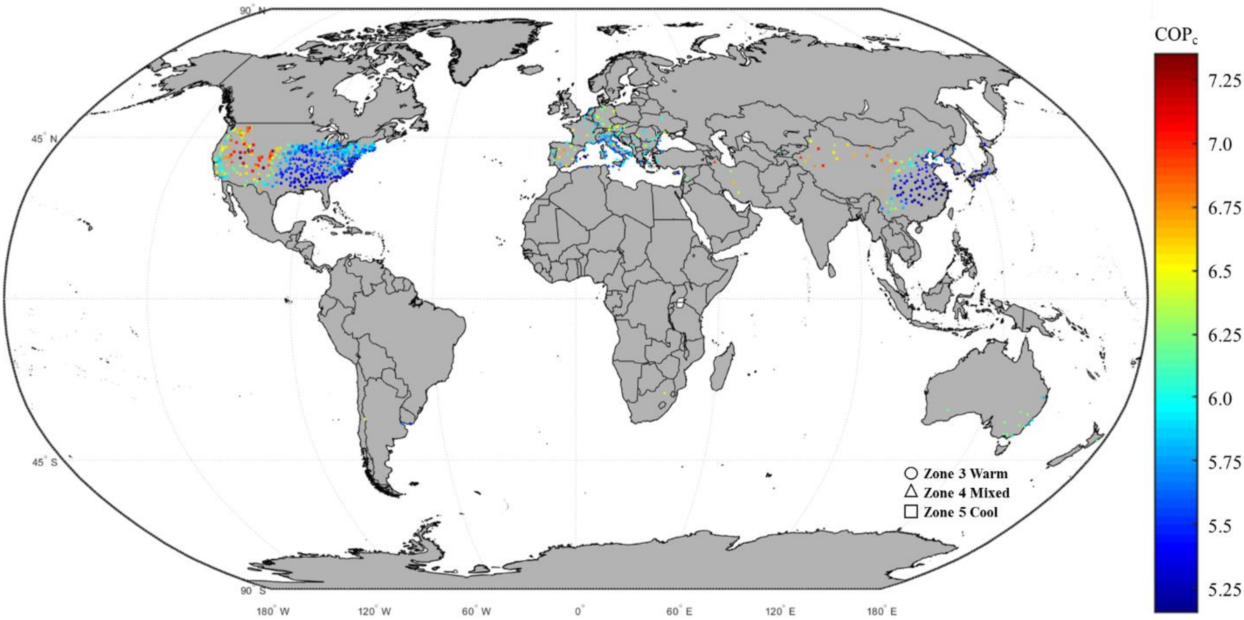

Fig. 7. COP$_c$ of HTHPs over the world

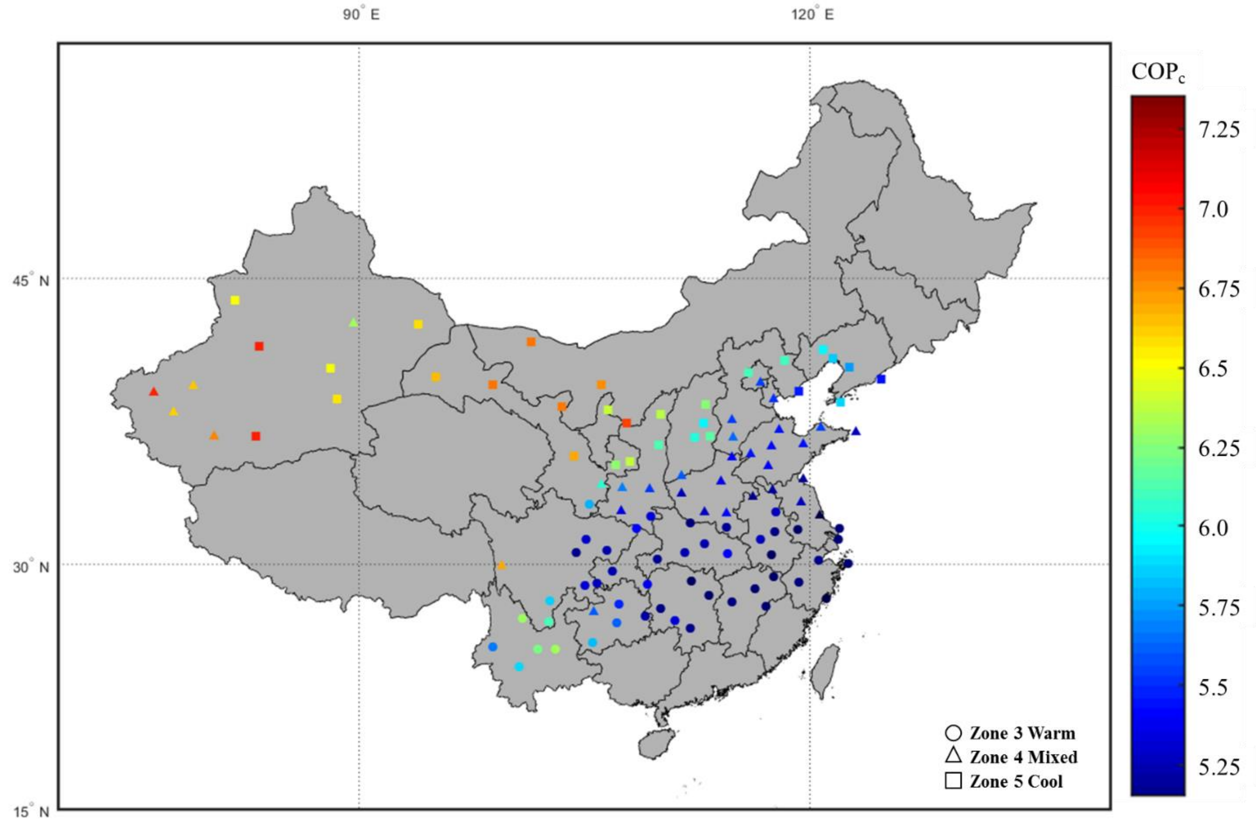

Fig. 8. COP_c of HTHPs in China

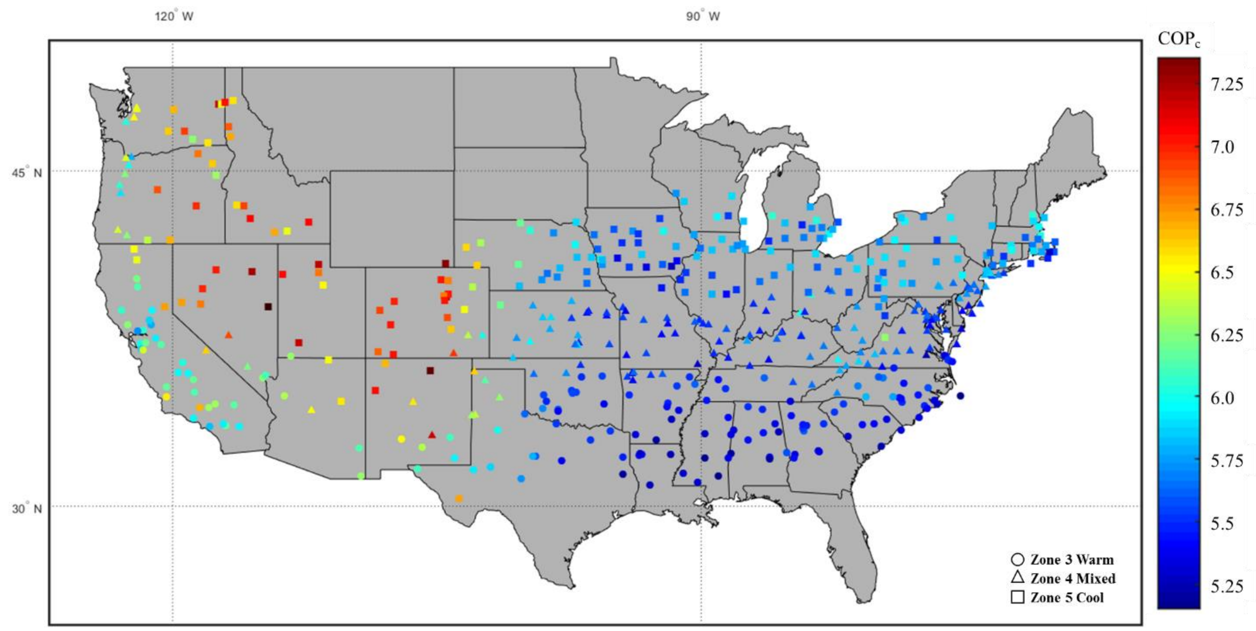

Fig. 9. COP_c of HTHPs in the USA

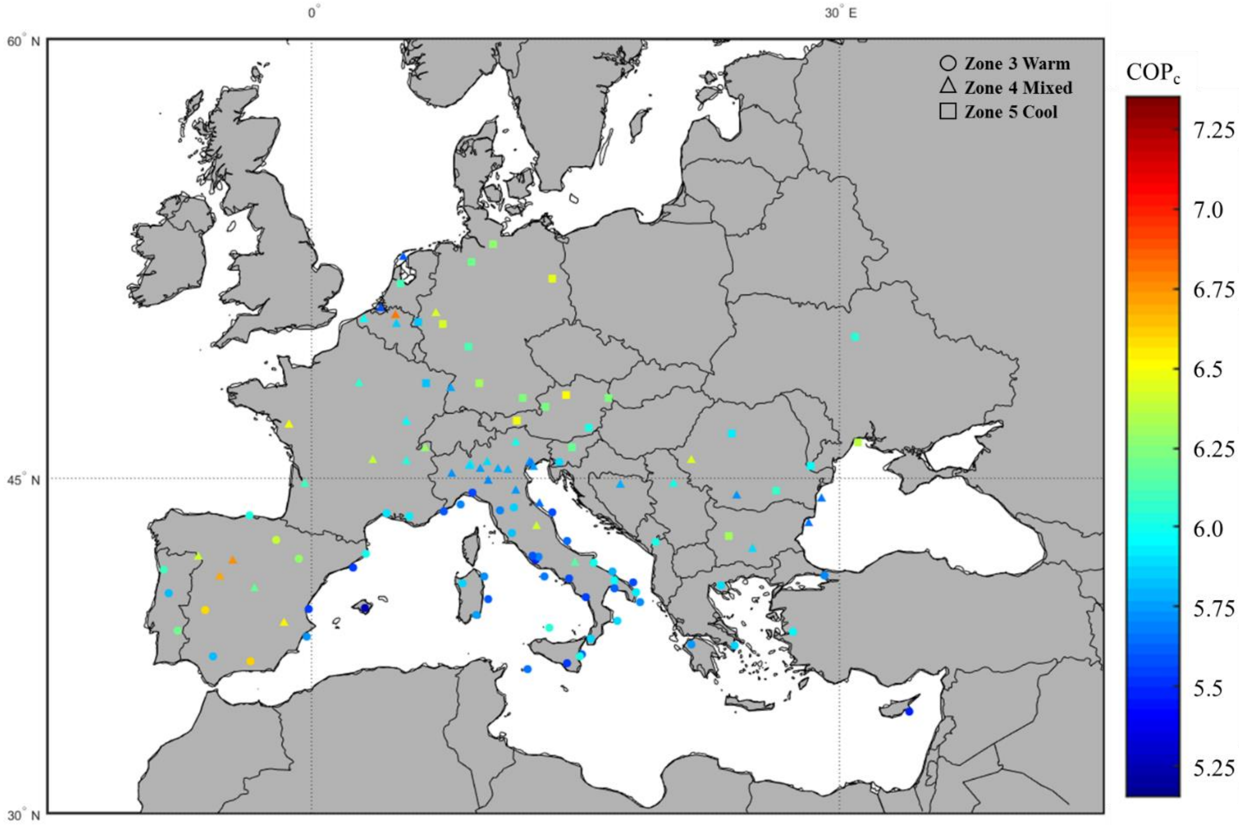

Fig. 10. COP$_c$ of HTHPs in Europe

4.2. Performance in heating season

The η_{RR} of the HTHPs which indicates the regeneration penalization (energy consumption of the regeneration device) in the heating season, is an important index. The η_{RR} of different locations varies from -33.2% to 34.0%, as presented in Fig. 11. When the η_{RR} is lager than zero, it means that the solution absorbs latent heat from the air and needs additional energy for solution regeneration. Although the absorbed latent can raise the solution temperature, the HTHP costs more electric energy by the regeneration device. In addition, the initial cost also increases with larger regeneration capacity. When the η_{RR} is less than zero, it means that the HTHP system can achieve the mass balance without addition regeneration. However, the evaporation of water reduces the temperature of the solution, which can reduce the efficiency of the system. Therefore, the locations whose η_{RR} is close to zero are considered to be better. These locations are marked in light green in Fig. 11, including east-central China, north-central of the USA. The mean relative humidity of these locations in heating season are around 70%. The locations in southwest China, west coast of the USA, and west Europe, have really high η_{RR}. Since the mean relative humidity of these locations in heating season are between 80% and 90%.

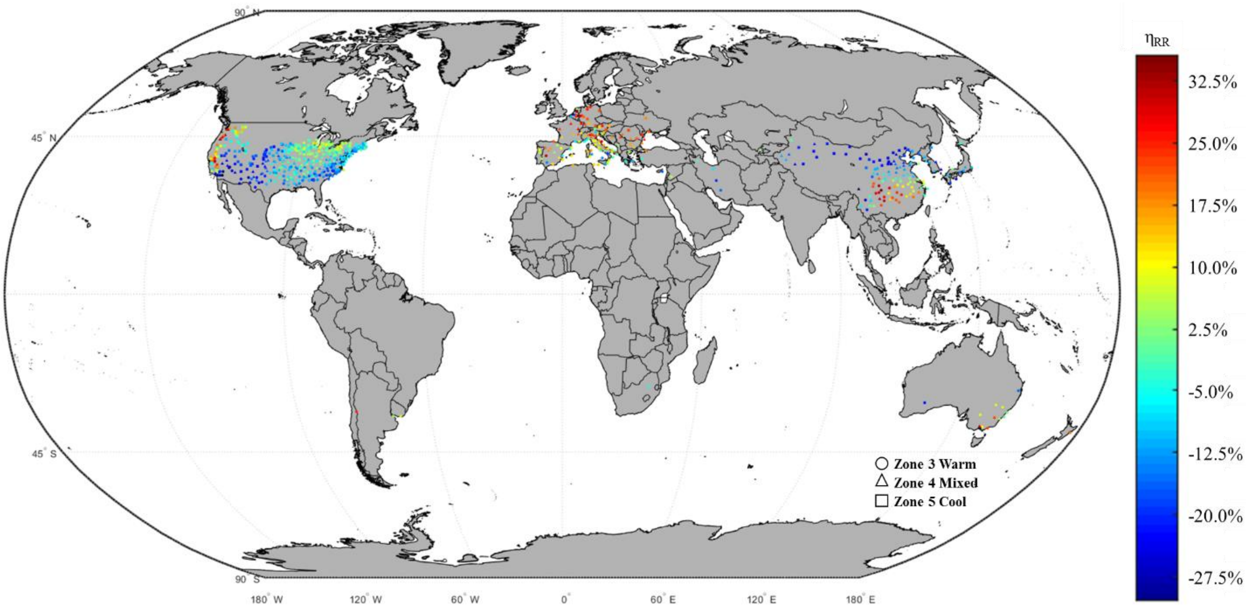

Fig. 11. η_{RR} of HTHPs over the world

The N_{UH} is another important index, which is defined as the number of hours when the heating capacity of the system cannot satisfy the building heating load. The higher N_{UH} means more energy cost by the auxiliary electric heater. Due to the energy storage of the solution (absorbing latent heat in the cold and humid hours, and self-regeneration in the warm and dry hours), the HTHP shows higher efficiency and capacity than the ASHP under severe operating conditions[5]. However, the HTHP still has high N_{UH} when applied in the north China, north-central and northeast of the USA, as shown in Fig. 12. Since these regions have really low temperature in the heating season. The N_{UH} of the locations with maritime climate (e.g. California of the USA, Yunnan province of China, Salamanca of Spain), is close to zero, since these locations have warm heating season.

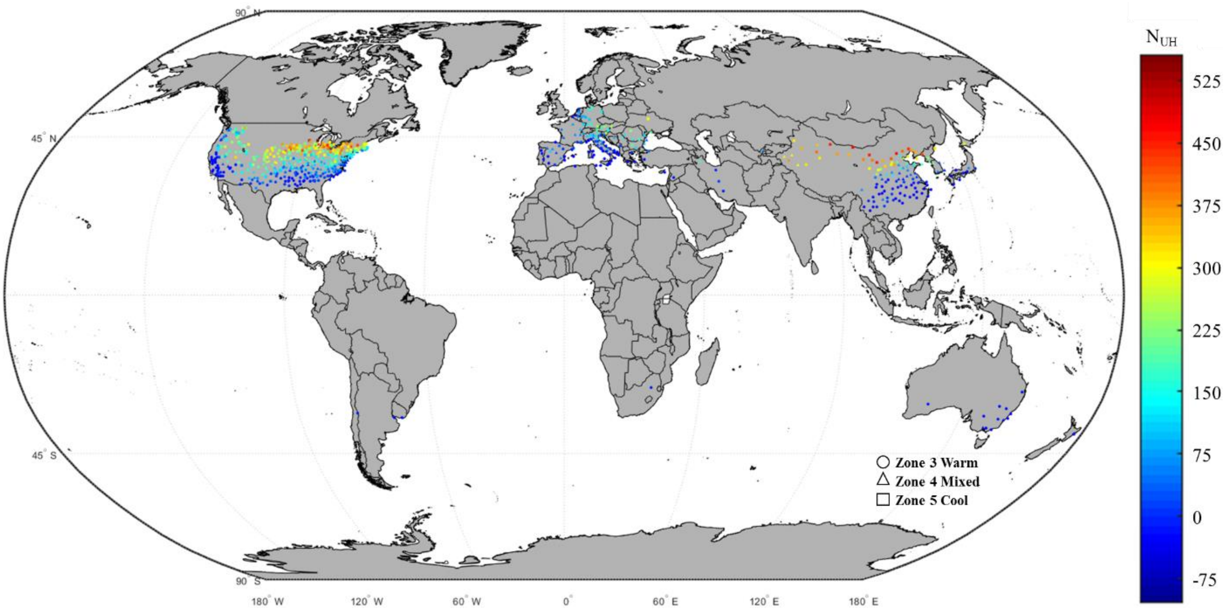

Fig. 12. N_{UH} of HTHPs over the world

The COP_h taking into account the energy consumption of the heat pump, regeneration device, and auxiliary electric heater, is a comprehensive index for evaluation of HTHP's performance in heating season. The COP_h of different locations varies from 2.24 to 4.12, as presented in Fig. 13 to Fig. 16. The COP_h decreases as the latitude increases, since the decrease of dry-bulb temperature can reduce the heat pump efficiency and increase N_{UH}. The average COP_h is 3.37 in Zone 3 (warm), 2.98 in Zone 4 (mixed), and 2.73 in Zone 5 (cool). The relative humidity can also have an influence on COP_h by affecting energy cost of regeneration and heat pump efficiency as well, as indicated in the analysis on η_{RR}. For instance, a comparation between Chongqing (HDD18°C is 1103) and Wenzhou (HDD18°C is 1106) are presented. These two locations have close latitudes and temperature, while the COP_h of Chongqing (2.83) is much lower than that of Wenzhou (3.72), as presented in Fig. 14. The mean relative humidity of Chongqing in heating season (86.4%) is much higher than that of Wenzhou (70.0%). As a result, the η_{RR} of Chongqing (34.1%) is much higher than that of Wenzhou (-1.3%), which means more energy consumption of regeneration for Chongqing. To present the results more clearly, the COP_h of locations in the USA are also demonstrated in Fig. 15.

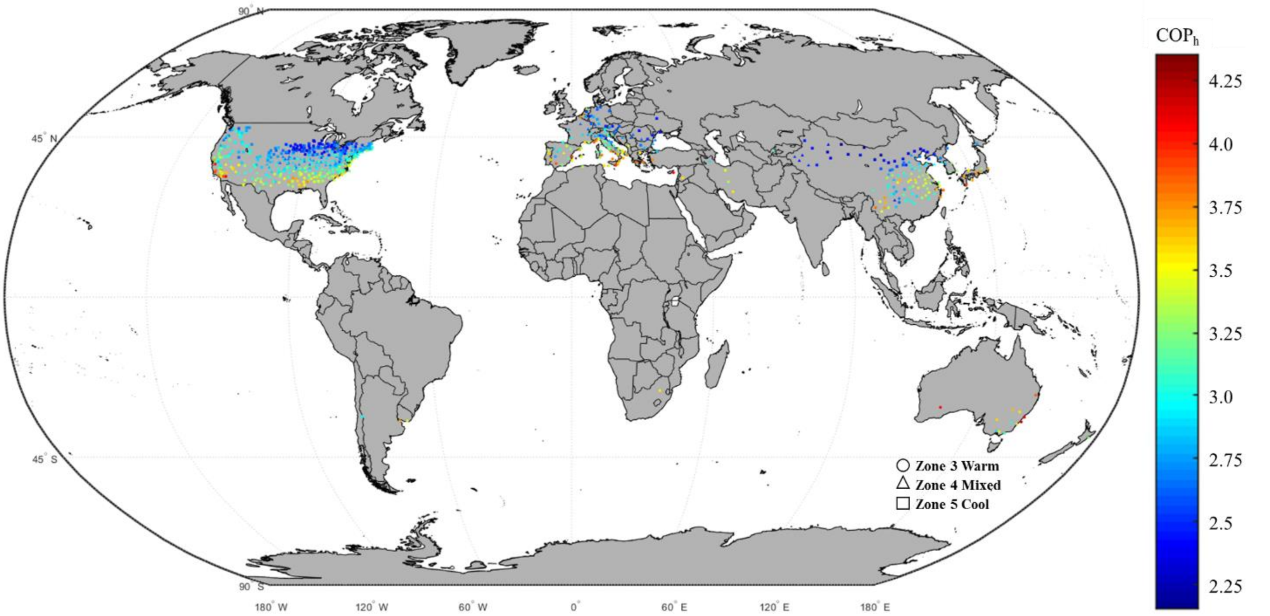

Fig. 13. COP_h of HTHPs over the world

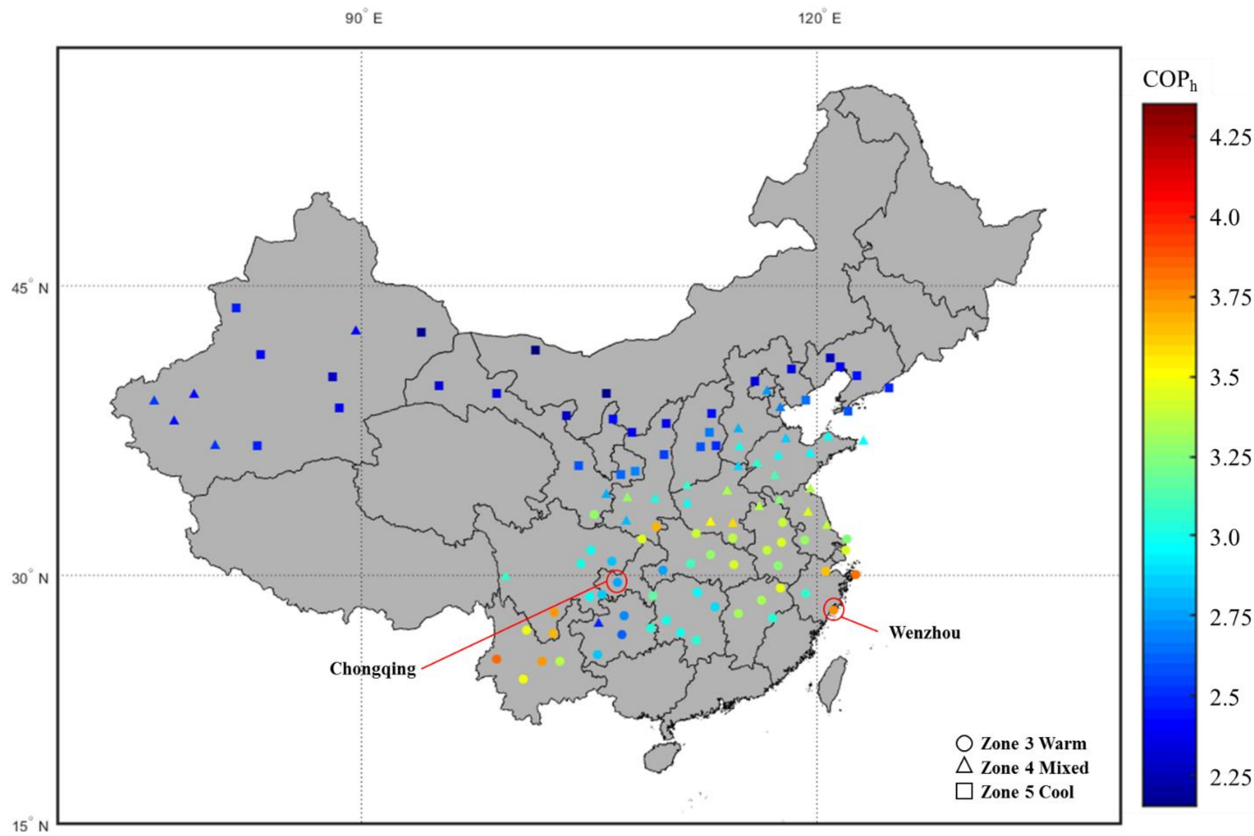

Fig. 14. COP$_h$ of HTHPs in China

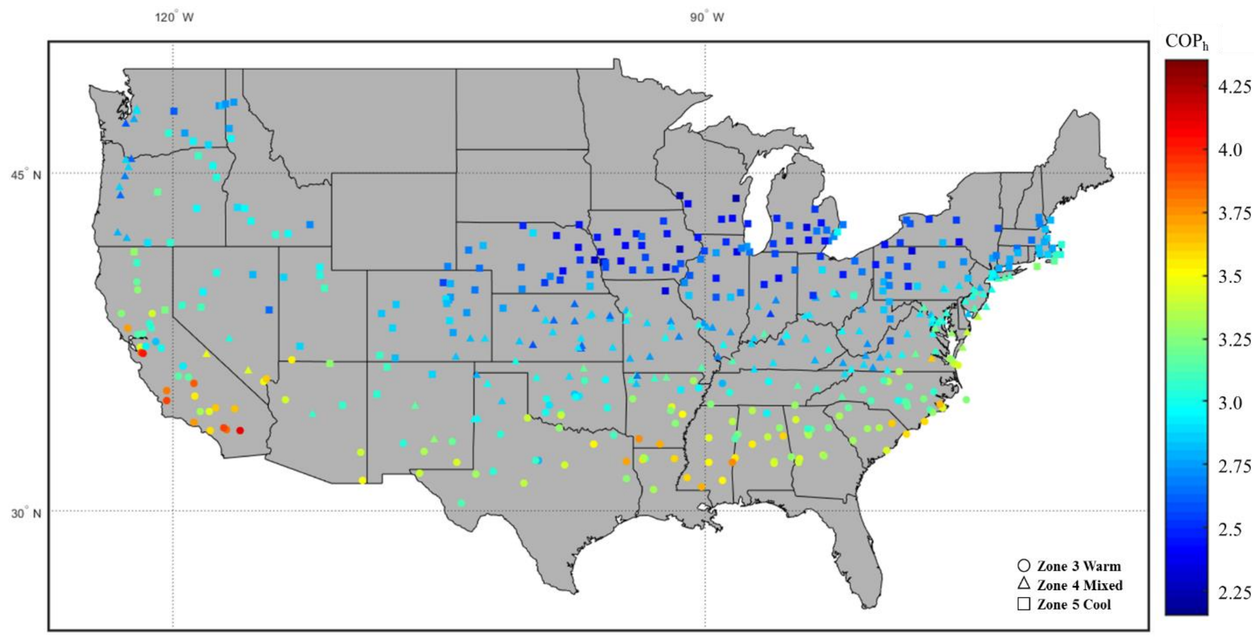

Fig. 15. COP$_h$ of HTHPs in the USA

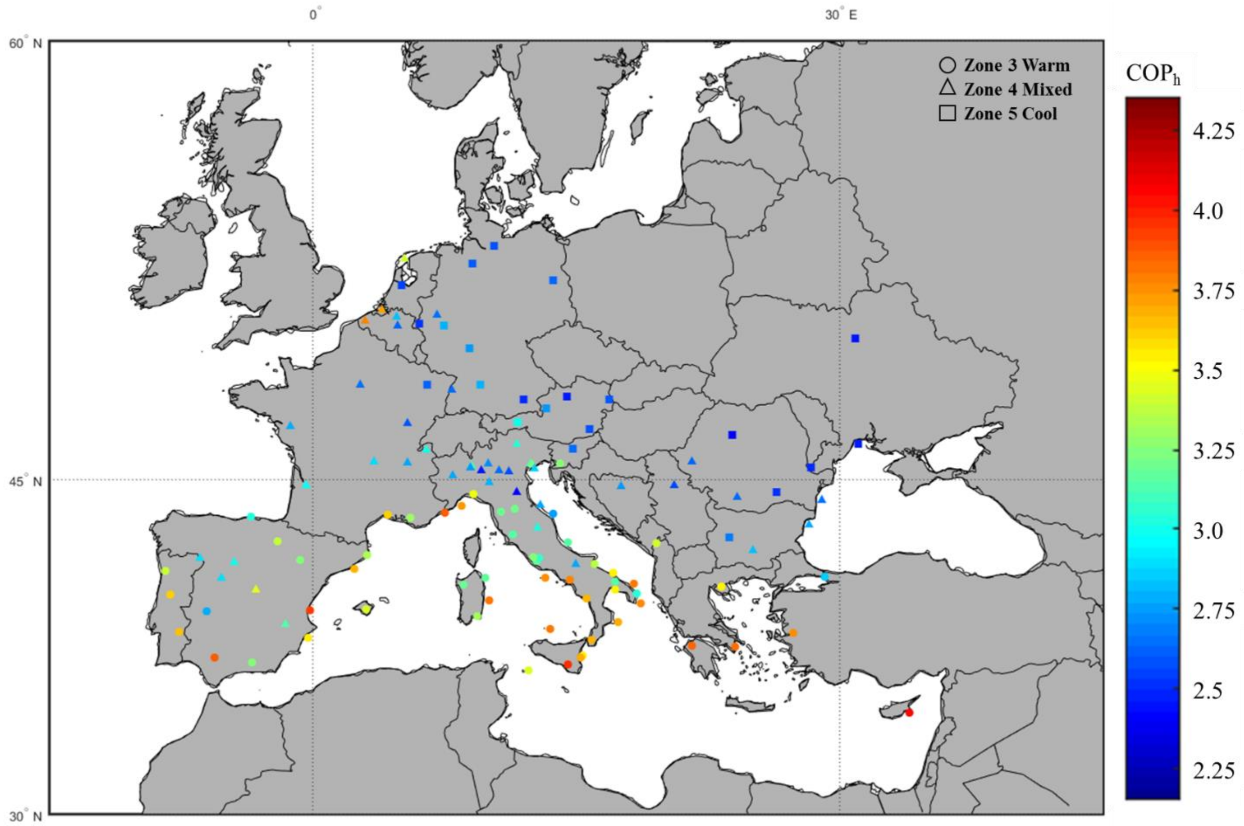

Fig. 16. COP$_h$ of HTHPs in Europe

4.3. Annual performance

Based on the results and analyses of the HTHP's performance in both cooling and heating seasons, the annual performance COP_a is calculated. Fig. 17 to Fig. 20 present the distributions of the COP_a, which varies from 2.46 to 6.10. This index is calculated by taking into consideration of total cooling supply, COP_c, total heating supply, and COP_h, as indicated in Eq.(32). According to the designed conditions mentioned in Section 3.3, the HTHPs in cooling season have lower condensing temperature and higher evaporating temperature than the heating season. Therefore, the COP_c is much higher than the COP_h as presented in Sections 4.1.1 and 4.1.2. As the latitude increases, the total cooling supply decreases and total heating supply increases, which means that the effect of COP_c decreases and the effect of COP_h increases. As a result, the distribution of the COP_a also follows the variation of latitude. The COP_a of Zones 3 to 5 are 4.67, 3.68, and 3.11, respectively. Specially, the locations with maritime climate (e.g. California of the USA, Yunnan province of China, southwest of Europe) has higher COP_a because these locations have cool cooling season and warm heating season.

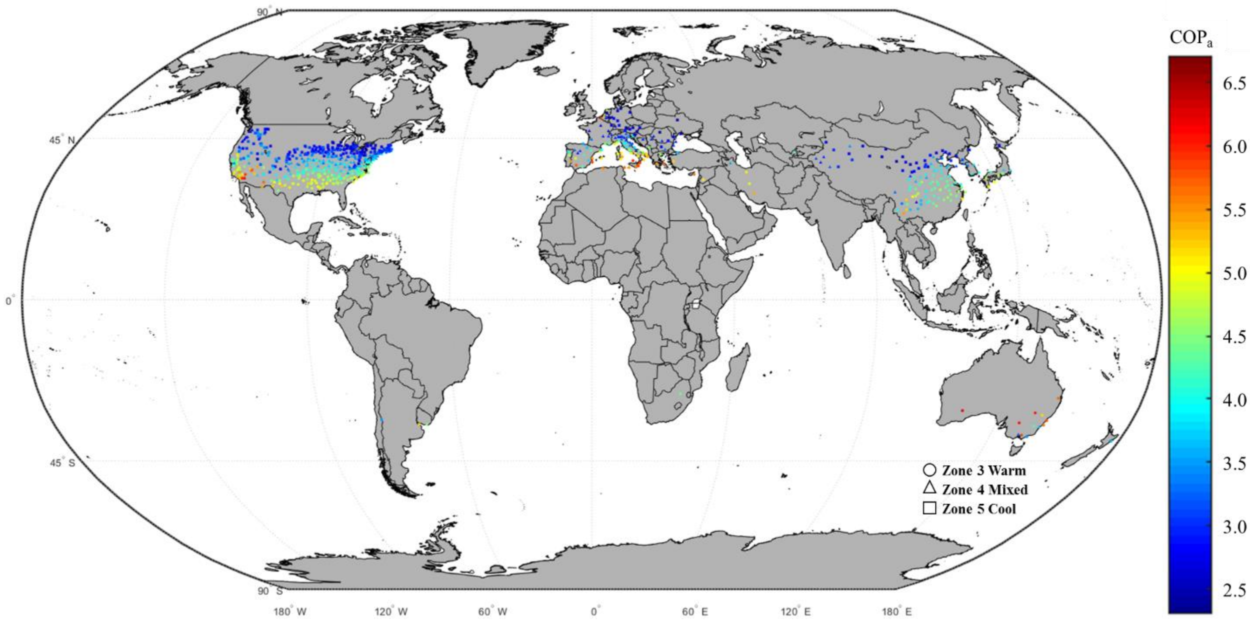

Fig. 17. COP$_a$ of HTHPs over the world

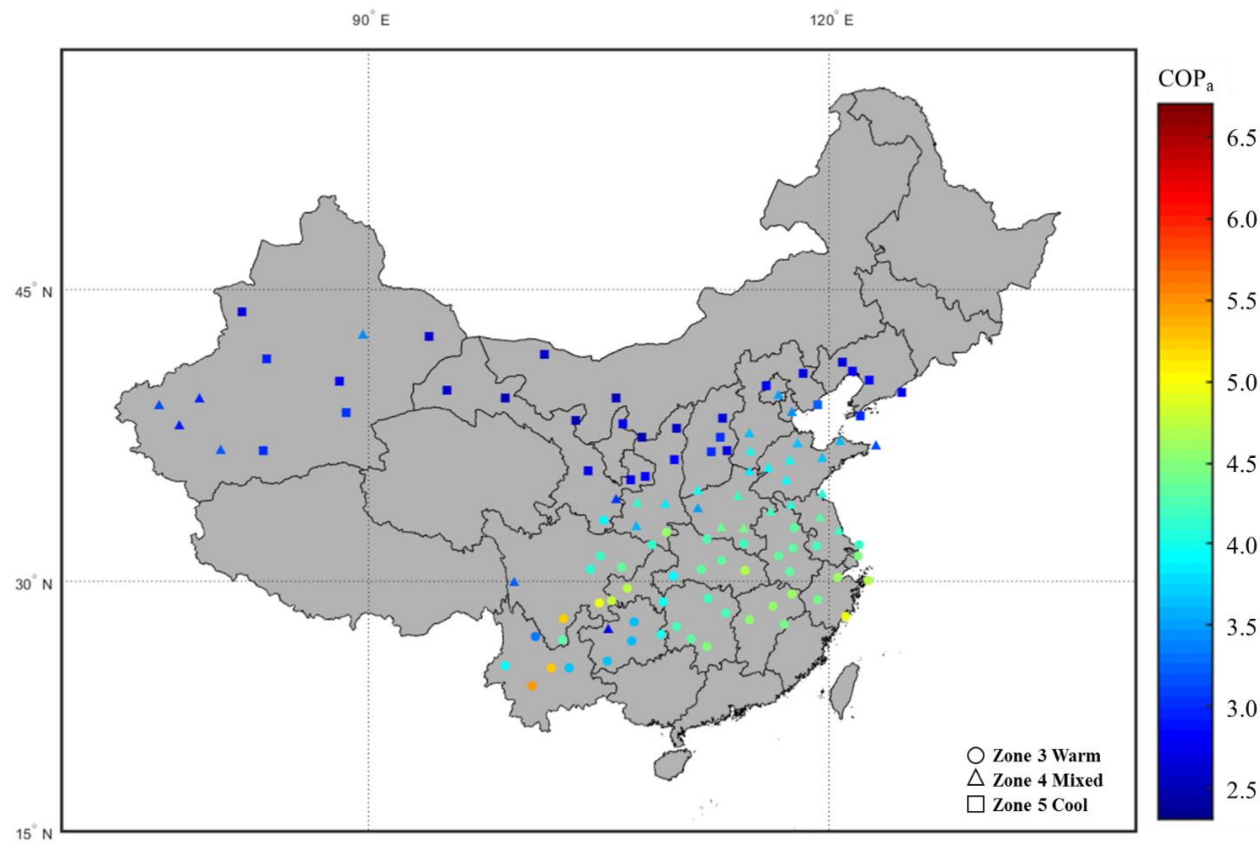

Fig. 18. COP$_a$ of HTHPs in China

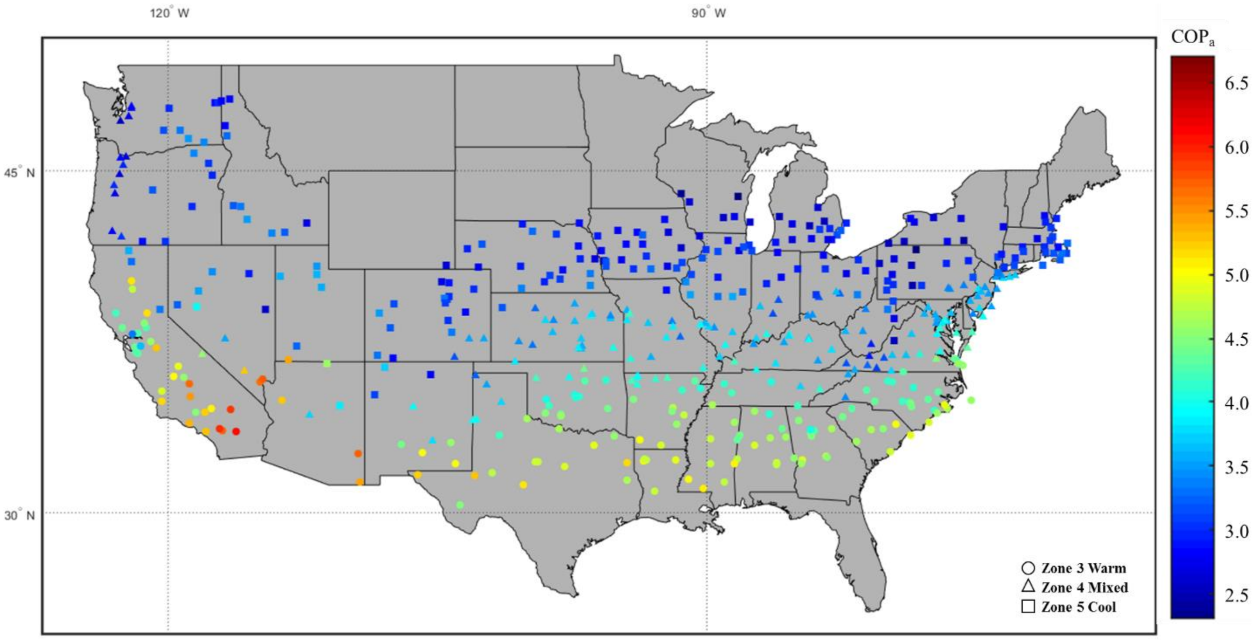

Fig. 19. COP$_a$ of HTHPs in the USA

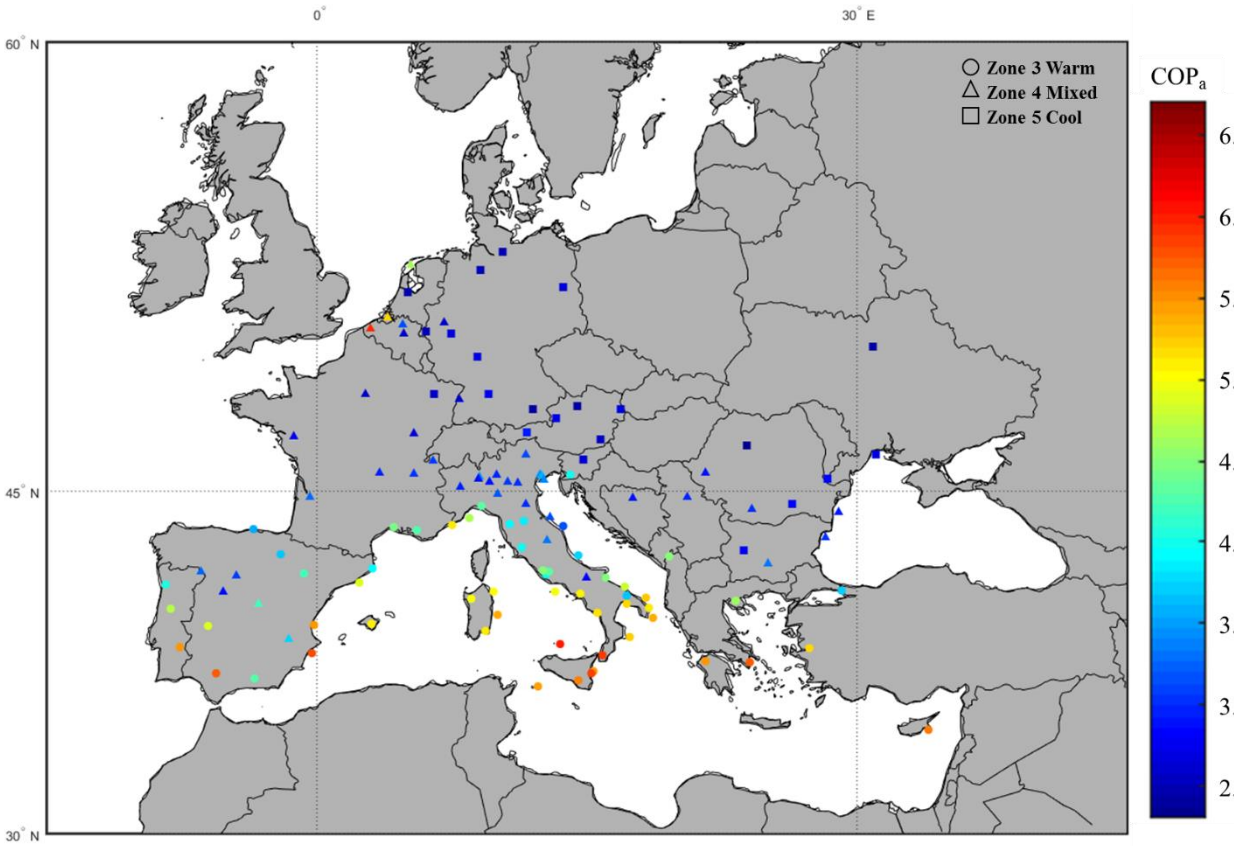

Fig. 20. COP$_a$ of HTHPs in Europe

4.4. Matching degree of the heat pump and heating tower

The above five indices focus more on the operational performance, while η_{MDHP} and η_{MDHT} can make contributions in the sizing and transformation process. For traditional heat pumps, such as ASHPs, the η_{MDHP} is usually larger than 1 in their applications, which means they are designed according to the cooling mode. However, the η_{MDHP} of the HTHPs has a much larger range when carrying out a large-scale evaluation. The results of η_{MDHP} and η_{MDHT} of different locations are presented in Fig. 21 and Fig. 22, respectively. The η_{MDHP} increases from 0.61 to 1.73 as the latitude increases. The locations with higher elevations (Colorado and Utah of the USA, Xinjiang and Gansu province of China) or maritime climate (e.g. California of the USA, Yunnan province of China, Salamanca of Spain) have lower η_{MDHT} than the other locations at the close latitude. When η_{MDHP} is larger than 1, it indicates that the heat pump should be sized according to the cooling mode in new HTHP system, or no add additional heat pumps is required in the transformation. When η_{MDHP} is less than 1, the conclusions are the opposite. The η_{MDHT} shows the similar distribution as η_{MDHP}, and the value varies from 0.48 to 1.34, which is smaller than η_{MDHP} in the same location. This is because the cooling capacity of the heating tower is much larger than its heating capacity, as indicated in Table 4. Similarly, the heating tower should be sized to satisfy the tower cooling load in new system, or no additional heating tower is required in transformation, when η_{MDHT} is larger than 1.

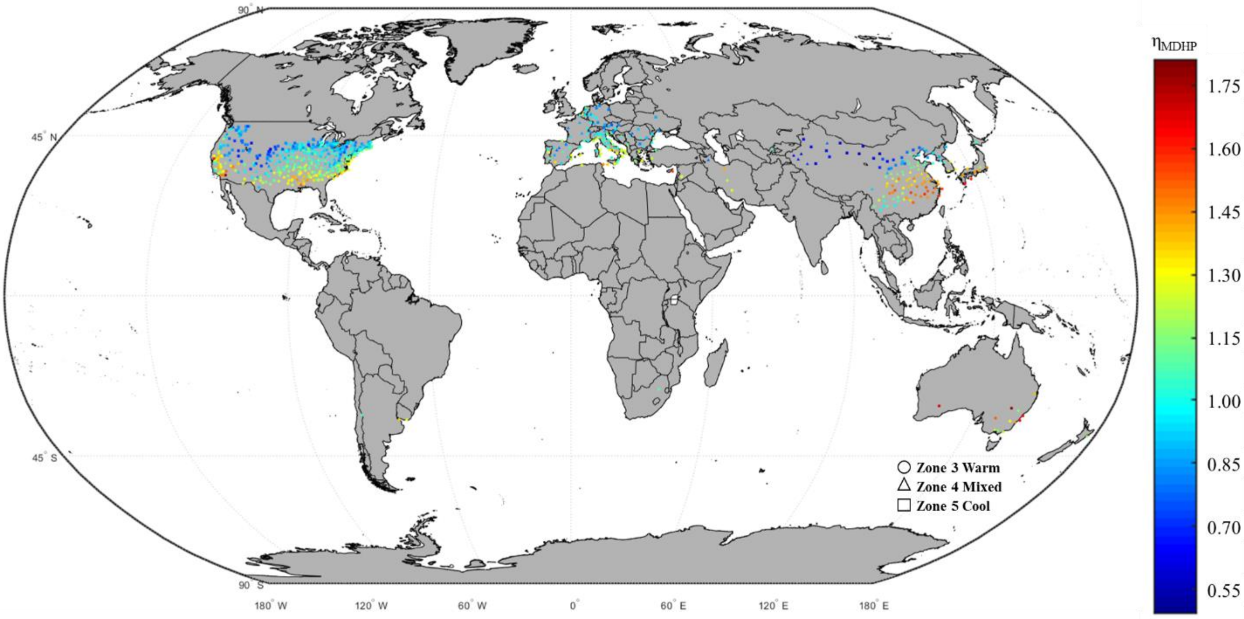

Fig. 21. η_{MDHP} of HTHPs over the world

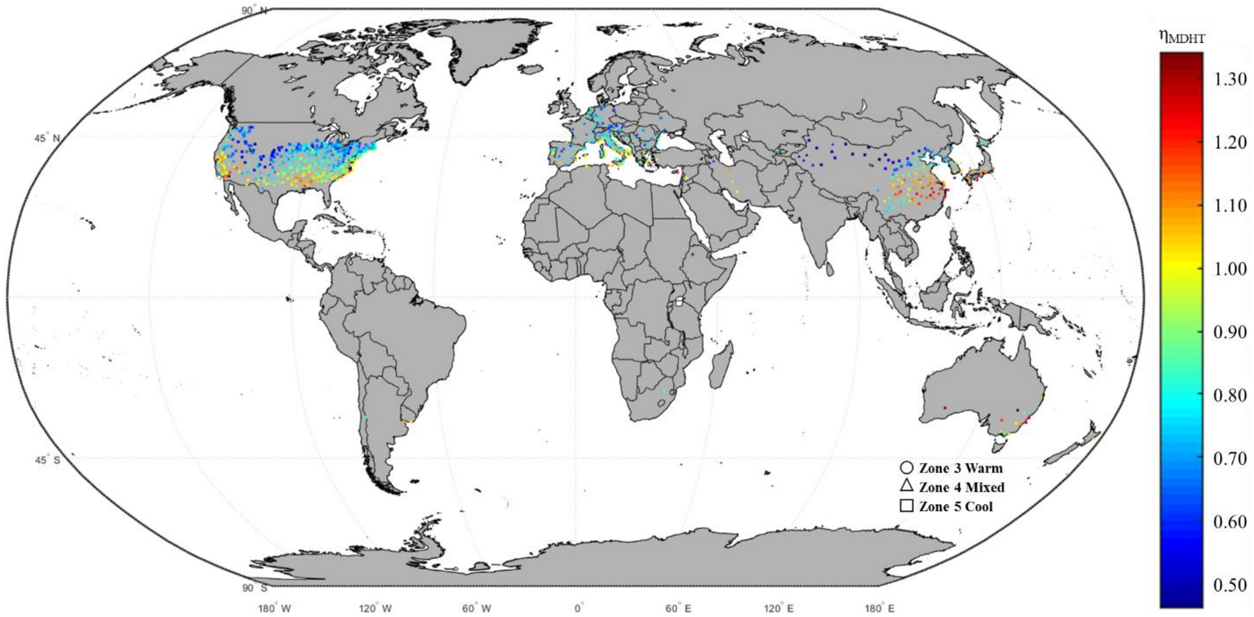

Fig. 22. η_{MDHT} of HTHPs over the world

5. Conclusion

Lacking performance evaluation of the HTHPs in different regions limits their applications worldwide. To address this problem, this paper carries out a large-scale comprehensive performance evaluation of the HTHP in 869 typical locations in the warm, mixed, and cool climate zones. The performance evaluation of the HTHPs is implemented by the processes of location selection, building load calculation, system sizing, simulation, and evaluation. Seven performance indices are adopted, and presented for all the selected locations. The main conclusions are summarized as follows:

(1) As the latitude increases, the COP_c increases from 5.13 to 7.40. The average COP_c is 5.73 in Zone 3 (warm), 5.83 in Zone 4 (mixed), and 6.14 in Zone 5 (cool). For the locations with close latitudes, these with high elevations or in maritime climate show higher COP_c.

(2) The η_{RR} of different locations varies from -33.2% to 34.0%, and is determined by relative humidity in heating season. The η_{RR} is around zero for the locations whose mean relative humidity in winter is about 70%, including east-central China and north-central of the USA. The locations whose mean relative humidity in winter is between 80% and 90% have really high η_{RR}, including southwest China, west coast of the USA, and west Europe.

(3) As the latitude increases, the COP_h of different locations decreases from 4.12 to 2.24. For the locations with close latitudes, these with maritime climate or low relative humidity have higher COP_h.

(4) As the latitude increases, the COP_a decreases from 6.10 to 2.46. The COP_as of Zones 3 to 5 are 4.67, 3.68, and 3.11, respectively. The results indicate that the HTHPs have excellent performance in Zone 3 (warm) and Zone 4 (mixed), and also can be applied in Zone 5 (cool).

(5) As the latitude increases, η_{MDHP} increases from 0.61 to 1.73, and η_{MDHT} increases from 0.48 to 1.34. The distributions of these two indices can direct the design of a new HTHP system or transforming of a chiller system into a HTHP system.

Acknowledgement

The research described in this paper is supported by the National Natural Science Foundation of China (No.51520105009), the China National Key R & D Program (No. 2016YFC0700305), and the Scientific Research Foundation of Graduate School of Southeast University (No. YBJJ1708). The research in the US is supported by the National Science Foundation (No. IIS-1802017).

Nomenclature

A	heat exchange area, m^2	λ	thermal conductivity coefficient, W m^{-1} K^{-1}
A_{th}	geometric throat area of the thermostatic expansion, m^2	ξ	coefficients of Eq.(18)
C_D	constant mass flow coefficient	ρ	density, kg m^{-3}
CDD10°C	cooling degree-day base 10°C, °C	ω	humidity ratio，kg kg^{-1}
COP_a	annual coefficient of performance, /	**Subscript**	
COP_c	cooling coefficient of performance, /	*a*	air
COP_h	heating coefficient of performance, /	*c*	condenser
Cp	specific heat capacity, kJ kg^{-1} K^{-1}	*chws/ chwr*	supply / return chilled water
G	mass flow flux， kg m^{-2} s^{-1}	*comp*	compressor
h	enthalpy, kJ kg^{-1}	*cws / cwr*	supply / return cooling water
h_c	heat transfer coefficient of tower, W m^{-2} K^{-1}	*DBC*	designed building cooling
h_d	mass transfer coefficient of tower, g m^{-2} s^{-1}	*DBH*	designed building heating
HDD18°C	heating degree-day base 18°C, °C	*e*	evaporator
K	heat exchange coefficient, kW m^{-2} ℃$^{-1}$	*EH*	electric heater
L	length of the packing, m	*HPC*	heat pump cooling
LMTD	logarithmic mean temperature difference, ℃	*HPH*	heat pump heating
M	mass flow rate, kg s^{-1}	*HTC*	heating tower cooling
m	mass flow rate in one element, kg s^{-1}	*HTH*	heating tower heating
N	rotation speed, Rev. min^{-1}	*hws / hwr*	supply / return hot water
N_{UH}	number of unsatisfactory hours, /	*i*	inlet or inner
P	pressure, Pa	*l*	liquid phase
Q	heat transfer capacity, kW	*lh*	latent heat
r	vaporization latent heat， kJ kg^{-1}	*m*	mean value of the inside and outside
R	Resistance of heat transfer, m^2 K W^{-1}	*MDHP*	matching degree of heat pump
T	temperature, ℃	*MDHT*	matching degree of heat pump
W	power consumption, kW	*o*	outlet or external
X	mass concentration of solution, /	*R*	refrigerant

Greek symbols		*rated*	performance under rated speed
α	coefficients of Eq.(1)	*RD*	regeneration device
α_w	specific area of the packing, m^2 m^{-3}	*RR*	regeneration ratio
β	coefficients of Eq.(2)	*s*	solution
γ	coefficients of Eq.(17)	*sh*	sensible heat
δ	thickness of the tube wall, m	*ss / sr*	supply / return solution
η_{MDHP}	matching degree of heat pump, /	*UH*	unsatisfactory hour
η_{MDHT}	matching degree of heat pump, /	*v*	vaper
η_{RD}	efficiency of the regeneration system, kg kWh^{-1}	*w*	water
η_{RR}	regeneration ratio, /	*wall*	wall of tube

References

[1] Kim M H, Kim H, Lee K S, et al. Frosting characteristics on hydrophobic and superhydrophobic surfaces: A review[J]. Energy Conversion and Management, 2017, 138: 1–11.

[2] Su W, Li W, Zhou J, et al. Experimental investigation on a novel frost-free air source heat pump system combined with liquid desiccant dehumidification and closed-circuit regeneration[J]. Energy Conversion and Management, 2018, 178(September): 13–25.

[3] Wang Z, Wang F, Ma Z, et al. Experimental performance analysis and evaluation of a novel frost-free air source heat pump system[J]. Energy and Buildings, 2018, 175: 69–77.

[4] Zhang S, Zhang L, Zhang X. Performance evaluation of existed ground source heat pump systems in buildings using auxiliary energy efficiency index: Cases study in Jiangsu, China[J]. Energy and Buildings, Elsevier B.V., 2017, 147: 90–100.

[5] Huang S, Zuo W, Lu H, et al. Performance comparison of a heating tower heat pump and an air-source heat pump: A comprehensive modeling and simulation study[J]. Energy Conversion and Management, 2019, 180: 1039–1054.

[6] Tan K, Deng S. A method for evaluating the heat and mass transfer characteristics in a reversibly used water cooling tower (RUWCT) for heat recovery[J]. International Journal of Refrigeration, 2002, 25(5): 552–561.

[7] Fujita T, Kawahara K. Thermal characteristics of heating tower part I: Counterflow towers[J]. Transactions of the Japan Society of Refrigerating and Air Conditioning Engineers, 2012, 6: 265–274.

[8] Fujita T, Kawahara K. Thermal characteristics of heating towers part II: Crossflow towers[J]. Transactions of the Japan Society of Refrigerating and Air Conditioning Engineers, 2012, 6: 275–284.

[9] Lu J, Li W, Li Y, et al. Numerical study on heat and mass transfer characteristics of the counter-flow heat-source tower (CFHST)[J]. Energy and Buildings, 2017, 145: 318–330.

[10] Wen X, Liang C, Zhang X. Experimental study on heat transfer coefficient between air and liquid in the cross-flow heat-source tower[J]. Building and Environment, 2012, 57: 205–213.

[11] Huang S, Lv Z, Liang C, et al. Experimental study of heat and mass transfer characteristics in a cross-flow heating tower[J]. International Journal of Refrigeration, 2017, 77: 116–127.

[12] Song P, Wang B, Li X, et al. Experimental research on heat and mass transfer characteristics of cross-flow closed-type heat-source tower[J]. Applied Thermal Engineering, 2018, 135: 289–303.

[13] Cui H, Li N, Wang X, et al. Optimization of reversibly used cooling tower with downward spraying[J]. Energy, 2017, 127: 30–43.

[14] Cui H, Li N, Peng J, et al. Investigation on the thermal performance of a novel spray tower with upward spraying and downward gas flow[J]. Applied Energy, 2018, 231: 12–21.

[15] Wu J, Zhang G, Zhang Q, et al. Artificial neural network analysis of the performance characteristics of a reversibly used cooling tower under cross flow conditions for heat pump heating system in winter[J]. Energy and Buildings, 2011, 43(7): 1685–1693.

[16] Zendehboudi A, Song P, Li X. Performance investigation of the cross-flow closed-type heat-source tower using experiments and an adaptive neuro-fuzzy inference system model[J]. Energy and Buildings, 2019, 183: 340–355.

[17] Liang C, Wen X, Liu C, et al. Performance analysis and experimental study of heat-source tower solution regeneration[J]. Energy Conversion and Management, 2014, 85: 596–602.

[18] Huang S, Lv Z, Zhang X, et al. Experimental investigation on heat and mass transfer in heating tower solution regeneration using packing tower[J]. Energy and Buildings, 2018, 164: 77–86.

[19] Ai S, Wang B, Li X, et al. Numerical analysis on the performance of mechanical vapor recompression system for strong sodium chloride solution enrichment[J]. Applied Thermal Engineering, 2018, 137: 386–394.

[20] Wen X, Cao X, Yu P, et al. Experimental Research on a Novel Solution Regeneration System for Heat Source tower Based on Vacuum Boiling and Condensation[J]. ES Energy & Environment, 2018, 2: 01–07.

[21] Liang C, Wen X, Zhang X. Construction and experimental research on heat pump system based on heat-source tower [J]. CIESC Journal, 2010, 61(s2): 142-146.

[22] Wu J, Zhang G, Zhang Q, et al. Experimental investigation of the performance of a reversibly used cooling tower heating system using heat pump in winter[J]. Asia-Pacific Power and Energy Engineering Conference, APPEEC, 2011, 43: 1685–1693.

[23] Zhang X, Wen X, Liang C. New type of dual high-efficiency heat pump system suited to hot summer and cold winter zones [J]. Refrigeration and air conditioning, 2013, 13(11): 6-10.

[24] Li N, Zhang W, Wang L, et al. Experimental study on energy efficiency of heat-source tower heat pump units in winter condition[C]//Proceedings - 3rd International Conference on Measuring Technology and Mechatronics Automation, ICMTMA 2011. 2011, 2: 135–138.

[25] Cheng J, Zou S, Chen S. Application Research on the Closed-loop Heat-source-Tower Heat Pump Air Conditioning System in Hot-summer and Cold-winter Zone[J]. Procedia Engineering, 2015, 121: 922–929.

[26] Chen W, Qu L, Wang C, et al. An experimental inverstigation of the performance of an air-source heat pump hot-water system based on saltwater energy towers [J]. Journal of Zhejiang University, 2012, 46: 1485-1489.

[27] Standard A. Performance Rating of Positive Displacement Carbon Dioxide Refrigerant Compressors and Compressor Units[S]Air-Conditioning, Heating, and Refrigeration Institute, 2013, 571.

[28] Winandy E, Saavedra C, Lebrun J. Experimental analysis and simplified modelling of a hermetic scroll refrigeration compressor[J]. Applied Thermal Engineering, 2002, 22: 107–120.

[29] Park N, Shin J, Chung B. A new dynamic heat pump simulation model with variable speed compressors under frosting conditions[C]//8th International Conference on Compressors and their Systems. 2013: 681–696.

[30] Eames I W, Milazzo A, Maidment G G. Modelling thermostatic expansion valves[J]. International Journal of Refrigeration, 2014, 38(1): 189–197.

[31] ASHRAE. ANSI/ASHRAE Standard 169-2013 - Climatic Data for Building Design Standards[S]American National Standards Institute, American Society of Heating, Refrigerating and Air-Conditioning Engineers, 2013: 98.